Scientific Report No. 75

SEM ANALYSIS OF LOSSLESS LOADED TRANSMISSION LINES

by

Ahmad Hoorfar and David C. Chang

June 1983

Electromagnetics Laboratory
Dept. of Electrical and Computer Engineering
University of Colorado
Boulder, Colorado 80309

This project is supported by the National Science Foundation
under Grant No. ECS-8021041.

SEM ANALYSIS OF LOSSLESS LOADED TRANSMISSION LINES

by

Ahmad Hoorfar and David C. Chang

Abstract

An SEM transient analysis of a lossless terminated transmission line as well as a transmission line with an arbitrarily-located load is presented. Extensive numerical results for the behaviors of the SEM poles in the complex frequency plane, their mode distributions along the line, and the final transient current responses are also presented. In addition, detailed physical explanations to some of the SEM modal behaviors, and their effects on the time-domain response, are provided. In particular, occurrence of degeneracies between the SEM modes and the existence of two different sets of natural modes on an off-center loaded line are discussed. Analogy between a loaded transmission line and a loaded thin-wire antenna is also noted.

Table of Contents

Table of Contents (cont)

1. INTRODUCTION

Transient on terminated transmission lines has been studied by many authors [1-5]. In general, there are three different methods available in analyzing the transients on a lossless terminated line [5]: the well-known series-method, Volterra integral equation method and the so-called singularity expansion method (SEM). These methods have been briefly compared by Tai in [5]. As has been concluded in [5], the SEM, compared to the other two methods, furnishes the complete solution without iteration, provided that the so-called SEM poles' singularities of the frequency domain response are available; and therefore it is inherently a more numerically efficient scheme for the design and synthesis of the late time response of an arbitrary-loaded transmission line [6, Appendix D].

Our study of the present problem however, is mainly motivated by our desire to interpret the SEM modal behaviors of a loaded thin-wire antenna [7]. The results obtained for the behaviors of the SEM poles and related mode distributions of a lossless loaded transmission line will facilitate that interpretation, and can provide some physical explanations for the modal as well as the transient behaviors of a loaded thin-wire antenna.

Presently, a general SEM solution does not seem to be available for a terminated transmission line with an arbitrarily located load. The SEM analysis in [5] is only given for a lossless transmission line terminated in one end with a load while the source and observation points are both located on the other end. Even for this rather simple case, no parametric study of the SEM poles, their modal distributions along the line or the final transient response, is given for a complex load. Few numerical results for the series R-L, R-C and R-L-C terminated lines are reported in [8]. However, those

results, which are presented for the SEM poles only, do not show the effect of the resistor R as it varies, and hence, do not lend themselves to the study of modal degeneracy.

Starting with the so-called telegraphist's equation, a systematic derivation of the SEM representation for an end-(impedance) terminated transmission line, is presented in section 2. Modal equation for the SEM poles (natural frequencies) as well as an explicit expression for the natural mode current of a lossless transmission line with an arbitrarily located load, is derived in section 3. Extensive numerical results for the natural frequencies and modes of various center as well as off-center loaded lines are presented in this section, and the occurrence of the modal degeneracies, for certain load combinations, are fully investigated. Finally in section 4, the corresponding SEM representation for the transient response of the loaded transmission line of section 3 is derived, and the numerical results for the transient responses are presented. A "critically-damped" transmission line is also defined in section 3 and its transient behavior is discussed in section 4.

2. ENDS-LOADED TRANSMISSION LINE; FORMULATION

Consider the lossless transmission line of Figure 1-a, which is driven by a pair of delta-function voltage generators, $\pm V_g(t)$, $V_g(t) = V_o H(t-t_o)$, located at $z = z'$. Defining the Fourier transformation pair as

$$\tilde{I}(\omega;z,z') = \int_{-\infty}^{\infty} I(t;z,z') e^{+i\omega(t-t_o)} dt \tag{1.1}$$

$$I(t;z,z') = \frac{1}{2\pi} \int_{-\infty}^{\infty} \tilde{I}(\omega;z,z') e^{-i\omega(t-t_o)} d\omega \tag{1.2}$$

the so-called telegraphist's equations for the current and voltage can therefore be written as [9]

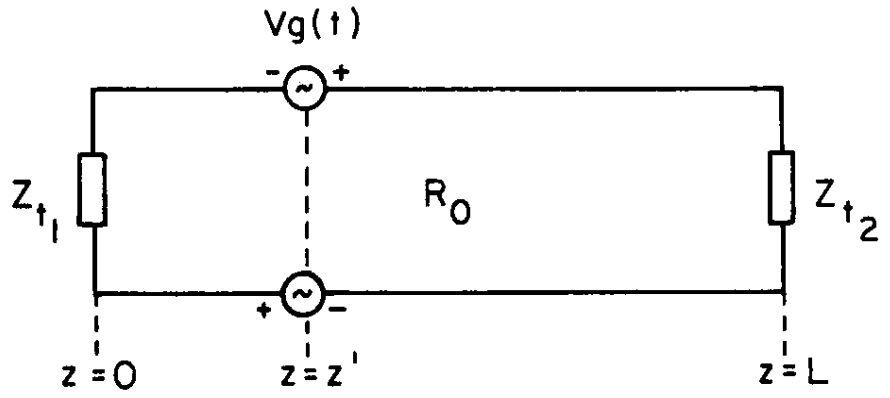

Fig. 1-a: Ends-loaded transmission line.

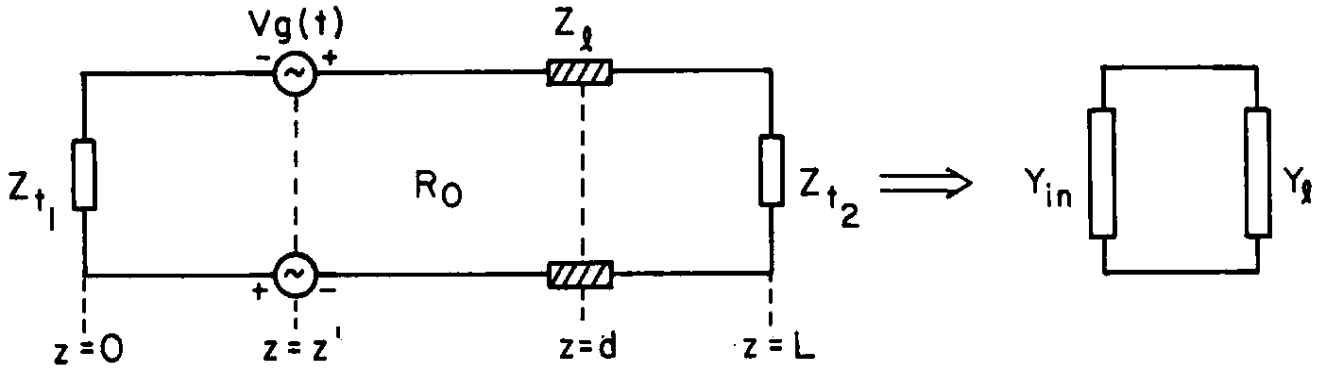

Fig. 1-b: Transmission line with an arbitrarily located load, and its equivalent resonant circuit.

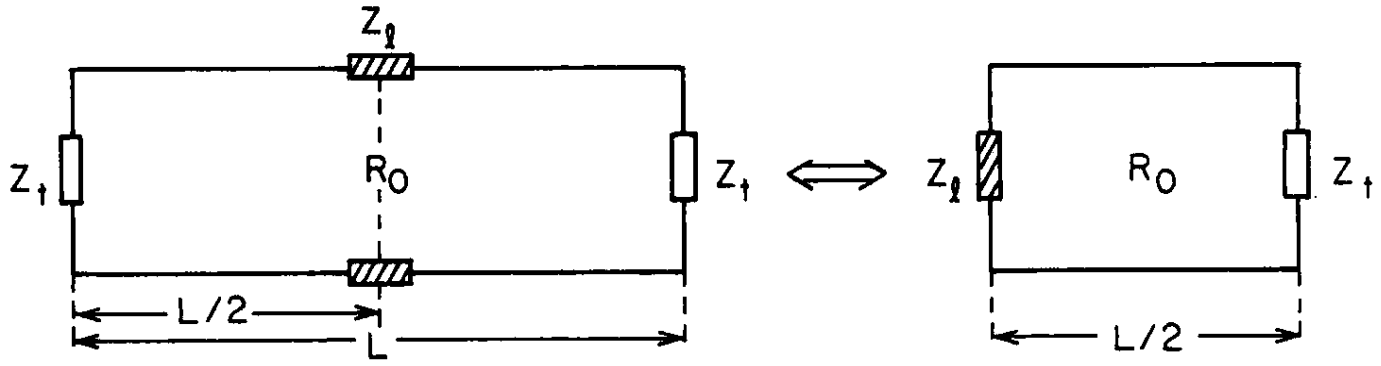

Figs. 1-c and 1-d: A symmetric-terminated center-loaded transmission line and its equivalent terminated line for even modes.

$$\begin{cases} \dfrac{d\tilde{I}}{dz} = (i\omega c_o)\tilde{V} \\ \dfrac{d\tilde{V}}{dz} = (i\omega \ell_o)\tilde{I} + i\,\dfrac{2V_o}{\omega}\,\delta(z-z') \end{cases} \quad ; \quad \begin{cases} \tilde{V}(\omega;0,z') = Z_{t1}\tilde{I}(\omega;0,z') \\ \tilde{V}(\omega;L,z') = Z_{t2}\tilde{I}(\omega;L,z') \end{cases}$$

(2) (3)

which immediately reduces to the following wave-equation for the current

$$\left(\frac{d^2}{dz^2} + \frac{\omega^2}{c^2}\right)\tilde{I} = -2C_oV_o\delta(z-z') \tag{4}$$

where $c = \dfrac{1}{\sqrt{\ell_o c_o}}$ is the velocity of propagation, and c_o and ℓ_o are the capacitance and inductance per unit length of the line, respectively.

Solution of (4) may be written as

$$\tilde{I}(\omega;z,z') = I_o(\omega)g_1(\omega;L-z_<)g_2(\omega;z_>) \tag{5}$$

where $z_{\substack{> \\ <}} \equiv \max_{\min}(z,z')$, and g_1 and g_2 are defined as the current distributions in the two regions $z < z'$ and $z > z'$, respectively. After invoking the end conditions, given in (3) at $z = 0$ and $z = L$, the following expression for g_1 and g_2 is obtained:

$$g_{1,2}(\omega;z) = e^{i\frac{\omega}{c}z} - \Gamma_{t_{1,2}}(\omega)e^{i\frac{\omega}{c}L}\,e^{i\frac{\omega}{c}(L-z)} \tag{6}$$

wherein the reflection coefficients Γ_{t_1} and Γ_{t_2} are given by

$$\Gamma_{t_{1,2}}(\omega) = \frac{Z_{t_{1,2}}(\omega) - R_o}{Z_{t_{1,2}}(\omega) + R_o} \quad ; \quad R_o = \sqrt{\frac{\ell_o}{c_o}} \tag{7}$$

The amplitude I_o in (5) is directly related to the source condition at $z = z'$.. The requirement from (4) that the derivative of $\tilde{I}$ has to have a jump of $-2c_oV_o$ at the source point, yields

$$I_o(\omega) = \left(\frac{iV_o}{\omega R_o}\right) \frac{e^{-i\frac{\omega}{c}L}}{\Delta(\omega)} \tag{8}$$

where

$$\Delta(\omega) = 1 - \Gamma_{t_1}(\omega)\Gamma_{t_2}(\omega)e^{i2\frac{\omega}{c}L} \tag{9}$$

After some rearrangement, the expression for the total current in (5) can be written alternatively as

$$\tilde{I}(\omega;z,z') = \frac{iV_o}{\omega R_o}\left\{e^{i\frac{\omega}{c}(z_>-z_<)} - \frac{1}{\Delta(\omega)}\left[\Gamma_{t_2}(g_1(\omega;L-z')e^{i\frac{\omega}{c}(L-z)} + \Gamma_{t_1}g_2(\omega;z')\, e^{i\frac{\omega}{c}z}\right]\right\} \tag{10}$$

Physically the first term represents the outgoing current wave from the source, while the second and third terms are the reflected waves away from the $z = L$ and $z = 0$ ends of the line, respectively.

It is evident from (5) and (8), that in addition to the pole, $\omega = 0$ of $\tilde{V}_g(\omega)$, the only other singularities of $\tilde{I}(\omega;z,z')$, in the complex ω-plane, are isolated at the SEM poles ω_s and $-\omega_s^*$ which are the solutions of

$$1 - \Gamma_{t_1}(\omega_s)\Gamma_{t_2}(\omega_s)e^{i2\frac{\omega_s}{c}L} = 0\ , \quad s = 0, 1, 2,... \tag{11}$$

It can be easily shown that the roots of (11) can exist only in the lower half of the complex ω-plane; this is consistent with the time causality principle for the time convention $e^{-i\omega t}$.

To find the time-domain response for the total current in (5), we now perform the Fourier inverse transformation, as given by (1.2). By deforming the contour of integration into the lower half of the ω-plane (Figure 2) for $t - t_o \geq \frac{z_> - z_<}{c}$, the residues at the poles of $\tilde{I}(\omega;z,z')$ are captured and finally we get

$$I(t;z,z') = \left(\frac{V_o}{R_o}\right)\left[P_o + \sum_{s=-\infty}^{\infty} \frac{\Gamma_1(\omega_s)}{\omega_s \Delta'(\omega_s)}\, G_s(z')G_s(z)e^{-i\omega_s(t-t_o)}\right] H\left(t-t_o - \frac{z_> - z_<}{c}\right) \tag{12}$$

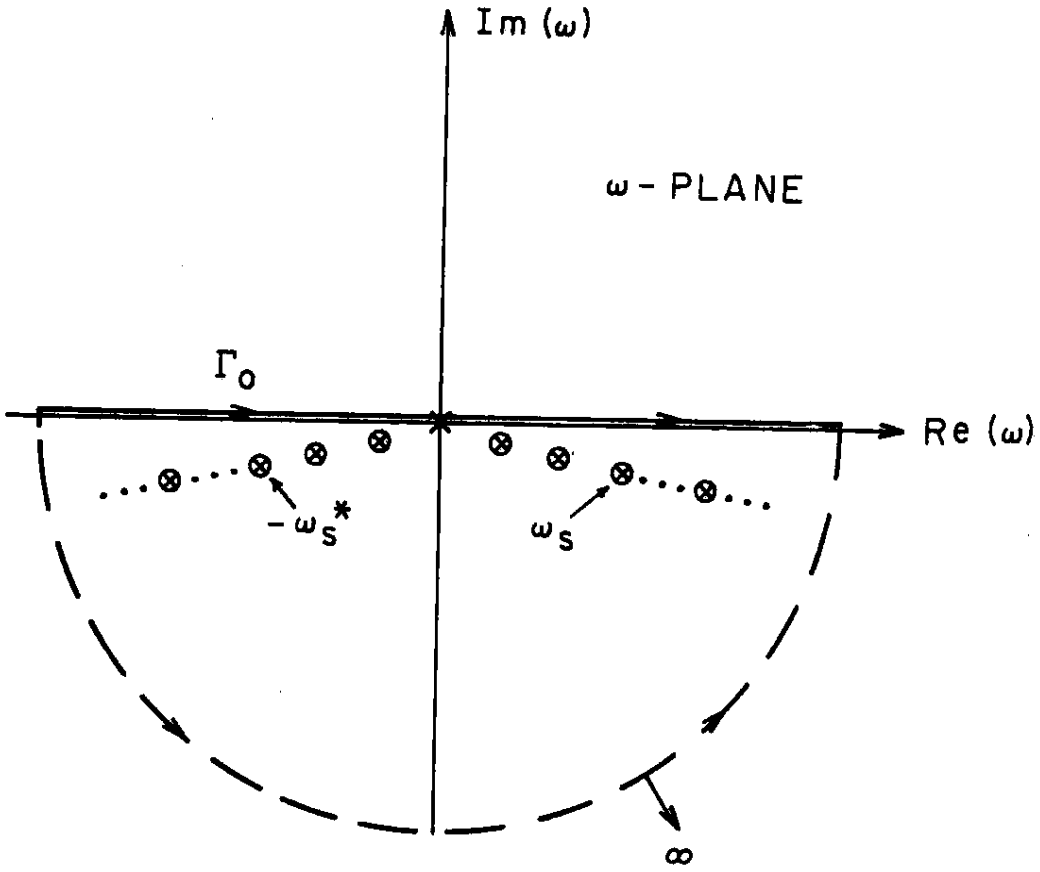

Fig. 2: Deformation of contour in the complex ω-plane.

where H is the unit-step function and P_o is the residue at the pole $\omega = 0$ of $\tilde{V}_g(\omega)$,

$$P_o = \frac{[1 - \Gamma_{t_1}(0)][1 - \Gamma_{t_2}(0)]}{1 - \Gamma_{t_1}(0)\Gamma_{t_2}(0)} \quad . \tag{13}$$

Also in (12)

$$\Delta'(\omega_s) = \frac{\Gamma'_{t_1}(\omega_s)}{\Gamma_{t_2}(\omega_s)} + \frac{\Gamma'_{t_2}(\omega_s)}{\Gamma_{t_1}(\omega_s)} + i2L/c \tag{14}$$

and $G_s(z)$ is the so-called natural mode current defined by

$$G_s(z) = e^{i\frac{\omega_s}{c}z} \pm \left(\frac{\Gamma_{t_1}(\omega_s)}{\Gamma_{t_2}(\omega_s)}\right)^{1/2} e^{i\frac{\omega_s}{c}(L-z)} \tag{15}$$

wherein + or - sign is chosen when s is odd or even, respectively. To obtain the transient response for the voltage one may now simply use

$$V(t;z,z') = -\frac{1}{c_o}\frac{d}{dz}\int_0^t I(t;z,z')dt' \tag{16}$$

where $I(t;z,z')$ is given by (12).

It should be mentioned here that the response in (12) could be derived from (6), through a more systematic SEM procedure by means of Mittag-Leffler theorem [10]. This procedure, which is given in Appendix A, expands the frequency-domain result of (5) in terms of the SEM poles before a transformation into the time-domain.

A comparison between the SEM representation on (12) and the transient formulation obtained by the so-called "series-method" in Appendix B, shows the advantages of the SEM in calculation of the "late-time" response. For the "early-time" response however, the series-method, which is based on the series expansion of $\Delta(\omega)$ in (5) and a term by term Fourier inverse transformation, will be more efficient as is discussed in Appendix B.

For the symmetric case of $Z_{t_1} = Z_{t_2} = Z_t$, the modal equation (11) and the natural mode current (15) reduce to

$$\Delta(\omega_s) = 1 - \Gamma_t^2(\omega_s) e^{i2\frac{\omega_s}{c}L} = 0 \ , \qquad \Gamma_t(\omega) = \frac{Z_t(\omega) - R_o}{Z_t(\omega) + R_o} \tag{17}$$

$$G_s(z) = e^{i\frac{\omega_s}{c}z} \pm e^{i\frac{\omega_s}{c}(L-z)}$$

$$= 2e^{i\omega_s\frac{L}{2c}} \begin{cases} \cos[\frac{\omega_s}{c}(z - \frac{L}{2})] & , \quad s \ \text{odd} \\ i \sin[\frac{\omega_s}{c}(z - \frac{L}{2})] & , \quad s \ \text{even} \end{cases} \tag{18}$$

It is worthy to note that for this symmetric case the expression in (12) is analogous to the SEM representation, given in [6], for the current response on a finite thin cylindrical antenna. For the antenna problem in [6] however, the corresponding G_s has a more complicated form which involves a function expressing the current on an infinite antenna, instead of exponential function in (18), and the corresponding $\Gamma_t(\omega_s)$ represents the reflection from the end of a semi-infinite antenna. Nevertheless, the transmission-line formulation of (12), (17) and (18) may be used to determine an approximate response for the current on a very thin-wire antenna, if one replaces the terminal impedance, Z_t, by an effective terminated function resulting from the radiation of the antenna (Z_{ta}), and R_o by the "antenna average characteristic impedance" (Z_{oa}). By using the expressions given by Schelkunoff [11] for Z_{ta} and Z_{oa}, Tai [8] has used this transmission-line model to calculate the natural frequencies (SEM poles) for a thin-cylindrical antenna. A numerical example, for the 1st-layer natural frequencies, in [8] shows however that the "transmission-line model" formulation for the antennas, (i.e., eq. (17) with $Z_t = Z_{ta}$ and $R_o = Z_{oa}$) without a suitable modification for the current distribution, is inadequate to yield a satisfactory result for the wire antennas, except for a very thin-wire antenna.

3. TRANSMISSION LINE WITH AN ARBITRARILY LOCATED LOAD

3.1 Natural Frequencies and Natural Mode Currents

3.1.1 Resonance condition. The ends-terminated transmission line of section 2, which is now loaded with an impedance $Z_\ell(\omega)$ located at z = d, is shown in Fig. 1-b. For this system the free current distribution on the line in the absence of any real source, can be written as

$$\tilde{I}_Z(\omega;z,d) = \tilde{V}_Z(\omega)Y(\omega;z,d) \tag{19}$$

where $\tilde{V}_Z(\omega) = -Z_\ell(\omega)\tilde{I}_Z(\omega;d,d)$ is a fictitious equivalent voltage generator located at z = d. In general, the "admittance" function $Y(\omega;z,z')$ is the normalized current at z on a "unloaded" (i.e., in the absence of the load Z_ℓ) transmission line due to a source at z'. Therefore by using the expression given in (5) for the current on an unloaded line, we may write

$$Y(\omega;z,z') = \frac{e^{-i\frac{\omega}{c}L}}{R_o\Delta(\omega)}\ f(\omega;z,z') \tag{20}$$

where $\Delta(\omega)$ is given by (9) and

$$f(\omega;z,z') = g_1(\omega;L-z_<)g_2(\omega;z_>) \tag{21}$$

wherein g_1 and g_2 are expressed in (6).

In order to obtain the resonance condition for the loaded transmission line, we now let z = d in (19) to yield the following modal equation

$$D(\omega_s^\ell) = 0\ ; \qquad s = 0,1,2,... \tag{22}$$

where

$$D(\omega) = \Delta(\omega) + \frac{Z_\ell(\omega)}{R_o}\left[e^{-i\frac{\omega}{c}L}\ f(\omega;d,d)\right] \tag{23}$$

Roots of (22), which can exist only in the lower half of the complex ω-plane, are the natural or resonance frequency, ω_s^ℓ , of the free current oscillations on the transmission line system. It is of significance to note that the

modal equation (22) could be physically interpreted as the resonance condition for the equivalent circuit shown in Fig. 1-b. In fact, free current in this circuit resonates at $\omega = \omega_s^\ell$ whenever

$$Y_\ell(\omega_s^\ell) + Y_{in}(\omega_s^\ell) = 0 \tag{24}$$

where $Y_\ell = \frac{1}{Z_\ell}$ and Y_{in} is the input admittance to the line at $z = d$. But by using eq. (5) and the definition of the input admittance, we have

$$Y_{in}(\omega) = \left.\frac{\tilde{I}}{\tilde{V}}\right|_{z=z'=d} = Y(\omega;d,d); \tag{25}$$

and consequently (24) is equivalent to (22), as expected.

The current distribution of the natural mode ω_s^ℓ is given by the free current (19) at $\omega = \omega_s^\ell$. Therefore, aside from a normalization factor, the natural mode current for a loaded transmission line is simply defined as:

$$\begin{aligned} F_s(z) &= f(\omega_s^\ell;z,d) \\ &= g_1(\omega_s^\ell;\ L - z_{d<})\ g_2(\omega_s^\ell;z_{d>}) \end{aligned} \tag{26}$$

where $z_{\substack{d> \\ <}} \equiv \min^{\max}(z,d)$. It is clear that, by using (9), the natural mode in (26) can also be expressed in terms of an outgoing current wave from the load, at $z = d$, and two reflected waves from the ends, at $z = 0$ and $z = L$.

A special case: For a center-loaded symmetric terminated transmission line, i.e. $d = \frac{L}{2}$ and $Z_{t_1} = Z_{t_2} = Z_t$, the modal equation (22) can be reduced to the following two equations:

$$1 - \Gamma_t(\omega_s)e^{i\frac{\omega_s}{c}L} = 0 \tag{27.1}$$

$$1 - \Gamma_t(\omega_s^\ell)\Gamma_\ell(\omega_s^\ell)e^{i\frac{\omega_s^\ell}{c}L} = 0 \tag{27.2}$$

where Γ_t and Γ_ℓ are the end and load reflection coefficients, respectively.

$$\Gamma_{t,\ell} = \frac{Z_{t,\ell}(\omega) - R_o}{Z_{t,\ell}(\omega) + R_o}$$

It is useful here to make some remarks regarding the equations in (27). As is evident the roots of equation (27.1) correspond to these natural modes which do not "see" and are not affected by the center-load. It is also interesting to note that the resonance condition in (27.2) is identical to that of a terminated line of Fig. 1-a, i.e. eq. (11), with $Z_{t_1} = Z_\ell$, $Z_{t_2} = Z_t$ and $L \to \frac{L}{2}$. Consequently, the (even) modes of the center-loaded line of Figure (1-c) are identical to the modes of the equivalent transmission line of Fig. 1-d. In general, the modal equations in (27) are transcendental equations which have to be solved numerically in order to obtain the natural frequencies ω_s^ℓ, $s = 0, \pm 1, \pm 2, \ldots$. For a resistive loaded and terminated line however, a simple analytical solution can be obtained. In fact for $Z_\ell = R_\ell$ and $Z_t = R_t$, we readily have

$$\left(\frac{L}{c\pi}\right)\omega_{2s} = 2s - \frac{j}{\pi}\ell n\left(\frac{R_t + R_o}{R_t - R_o}\right) \qquad (28.1)$$

$$s = 0, \pm 1, \pm 2, \ldots$$

$$\left(\frac{L}{c\pi}\right)\omega^\ell_{2s-1} = 2s - 1 - \frac{j}{\pi}\left[\ell n\left(\frac{R_t + R_o}{R_t - R_o}\right) + \ell n\left(\frac{R_o + R_\ell}{R_o - R_\ell}\right)\right] \qquad (28.2)$$

In the next section we will discuss this special case and also present numerical results for the solutions of the modal equations (27) and (22), for various $Z_\ell(\omega)$ and d.

3.1.2 Natural frequencies of a loaded, open-circuit transmission line. We now present some numerical examples for the natural frequencies and the corresponding natural modes distributions of a center as well as an off-center loaded lossless transmission line. For simplicity, the results which will be discussed here are obtained for a symmetric open-circuit terminated line, i.e., $Z_{t_1} = Z_{t_2} \to \infty$ and consequently $\Gamma_{t_1} = \Gamma_{t_2} = +1$. The modal

equation (22) and the natural mode distribution (26) can then be simplified to

$$\sin(\omega_s^{\ell}\frac{L}{c}) - 2\frac{Z_{\ell}(\omega_s^{\ell})}{R_o}\sin(\omega_s^{\ell}\frac{d}{c})\sin(\omega_s^{\ell}(L-d)/c) = 0 \tag{29}$$

$$F_s(z) = (4e^{i2\frac{\omega_s^{\ell}}{c}L})\sin(\frac{\omega_s^{\ell}}{c}z_{d<})\sin[\frac{\omega_s^{\ell}}{c}(L-z_{d>})] \tag{30}$$

In addition to the simplicity of calculations, our interest in this special case stems from our desire to interpret and justify the SEM properties of a thin-wire cylindrical antenna [7]. In fact, because the end-reflection coefficient of a thin-wire antenna indeed approaches +1 as the wire radius approaches zero [6], a loaded transmission line with open ends will provide some specific information about the nature and behavior of the natural frequencies and mode distributions of a thin-wire antenna.

Natural frequencies of a center-loaded transmission line

In the first set of results, natural frequencies of a center-loaded transmission line will be presented. The corresponding resonance condition is given by eqn. (29) with $d = \frac{L}{2}$, or more explicitly by the set of equations on (27) with $\Gamma_t = +1$. Then, the first equation in (27) has the zeroes at

$$(\frac{L}{c\pi})\omega_{2s} = 2s \quad , \quad s = 0, \pm 1, \pm 2, \ldots \tag{31}$$

which correspond to the natural modes, with odd distributions in z, that are not affected by the load. We now discuss solutions of eq. (27.2):

a) Purely resistive load, i.e. $Z_{\ell} = R_{\ell}$:

As was discussed earlier, for a resistive-loaded line the second equation in (27) has solutions which are given by (28.2), or more explicitly

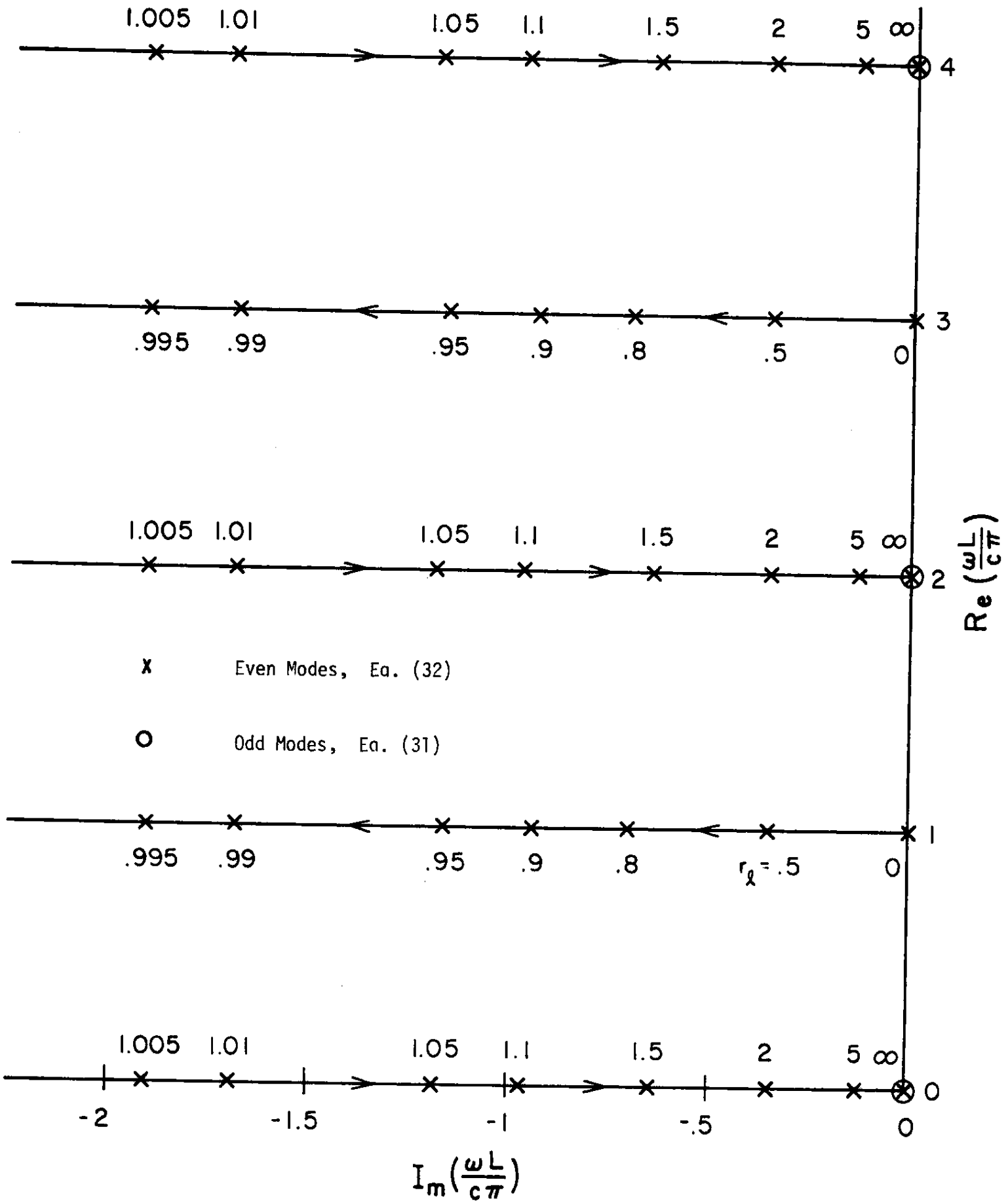

Fig. 3: Variation of the natural frequencies of a resistively center-loaded transmission line as a function of $r_\ell = R_\ell/R_o$.

$$\begin{cases} \left(\frac{L}{c\pi}\right)\omega_{2s-1}^{\ell} = 2s-1-\frac{j}{\pi}\ell n\left(\frac{1+r_\ell}{1-r_\ell}\right), & r_\ell < 1 \qquad (32.1) \\ \qquad\qquad s = 0, \pm 1, \pm 2, \ldots \\ \left(\frac{L}{c\pi}\right)\omega_{2s}^{\ell} = 2s-\frac{j}{\pi}\ell n\left(\frac{r_\ell+1}{r_\ell-1}\right), & r_\ell > 1 \qquad (32.2) \end{cases}$$

where $r_\ell = \frac{R_\ell}{R_o}$. These natural frequencies in the complex ω-plane are shown in Figure 3, as the normalized resistive load, r_ℓ, varies from 0 to ∞. As can be seen in (32) and the figure, in addition to the conjugate poles at ω_s^{ℓ} and $-\omega_s^{\ell *}$, $s \geq 1$, there is a single ω_o^{ℓ} pole located on the imaginary axis. This so-called "evanescent-mode" exists for $r_\ell > 1$. As $r_\ell \to 1$, $I_m(\omega_s^{\ell}) \to \infty$ and therefore as r_ℓ increases for $1-\varepsilon$ to $1+\varepsilon$ ($\varepsilon > 0$) it is not possible to determine whether $\omega_{2s-1}^{\ell} \to \omega_{2s}^{\ell}$ or $\omega_{2s-1}^{\ell} \to \omega_{2s-2}^{\ell}$. This difficulty is due to the uncertainty in choice of the logarithmic branch in (32) for this idealized pure resistive case. It can easily be shown from (32) however, that if r_ℓ has an imaginary part, i.e. $r_\ell + i\delta$, then choice of the principal value of the logarithmic function in (32) yields

$$\omega_{2s-1}^{\ell} \to \omega_{2s}^{\ell}, \quad \delta > 0 \qquad (33.1)$$

$$\omega_{2s-1}^{\ell} \to \omega_{2s-2}^{\ell}, \quad \delta < 0 \qquad (33.2)$$

as r_ℓ varies from 0 to ∞. Consequently for a load with $R_\ell - C_\ell$, i.e. $R_\ell C_\ell$ in series, or $R_\ell - L_\ell$, i.e. $R_\ell L_\ell$ in series, the corresponding natural frequencies are expected to behave like (33.1) or (33.2), accordingly.

b) Resistive load in series with a capacitance ($R_\ell - C_\ell$) or an inductance ($R_\ell - L_\ell$):

By numerically solving eq. (27.2), the natural frequencies of the various center-loaded transmission line are obtained and shown in Figures (4-8). The results for the series $R_\ell - C_\ell$ and $R_\ell - L_\ell$ loads are plotted in Figs. 4 and 5,

respectively. In these figures the capacitance or the inductance is normalized to give an impedance value of $x_C = 0.1$ and 1.0 or $x_L = 0.1$ and 1.0 at the frequency of $\omega = \frac{c\pi}{L}$. As can be seen, the natural frequencies of these transmission lines vary from ones corresponding to the symmetric modes of a line of length L when $r = 0$ to ones corresponding to a line having half of the length, i.e. $\frac{L}{2}$ when $r \to \infty$. In this transition the natural frequencies ω_s^ℓ, pass through "turning" points with maximum attenuation (i.e., where $|I_m(\omega_s^\ell)|$ is maximum). As r $(= \frac{R_\ell}{R_o})$ increases from 0 to ∞ however, the natural frequencies of the R_ℓ - C_ℓ loaded line move upward in the complex ω-plane (i.e., $I_m(\omega_{2s-1}^\ell) \to 2s$), whereas those of the R_ℓ - L_ℓ loaded line move downward (i.e., $I_m(\omega_{2s-1}^\ell) \to 2s - 2$), as was discussed earlier for a slightly reactive load. For the R_ℓ - C_ℓ loaded line in Figure 4, the first natural frequency moves upward in the ω-plane and coincide with the second (odd) mode (i.e., ω_2 in (31)), as r approaches infinity. Like in the case of a resistively loaded line, there is always an evanescent mode located on the imaginary axis for $1 < r < \infty$.

The situation for a resistance in series with an inductance is quite different, however. For the R_ℓ-L_ℓ loaded case, as r increases, the first natural frequency approaches the negative imaginary axis, forms a degenerate mode (i.e., a <u>double</u> SEM pole) there with its conjugate pair, $-\omega_1^{\ell *}$, and then the two poles split apart and move in the opposite directions along the negative imaginary axis and finally approach $-i0$ and $-i\infty$ as $r \to \infty$. In general the double pole which occurs for a "critical" value of resistor $r = r_c$, satisfies the condition that the derivation of the modal equation also vanishes, i.e.

$$D'(\omega_c^\ell) = 0 \tag{34}$$

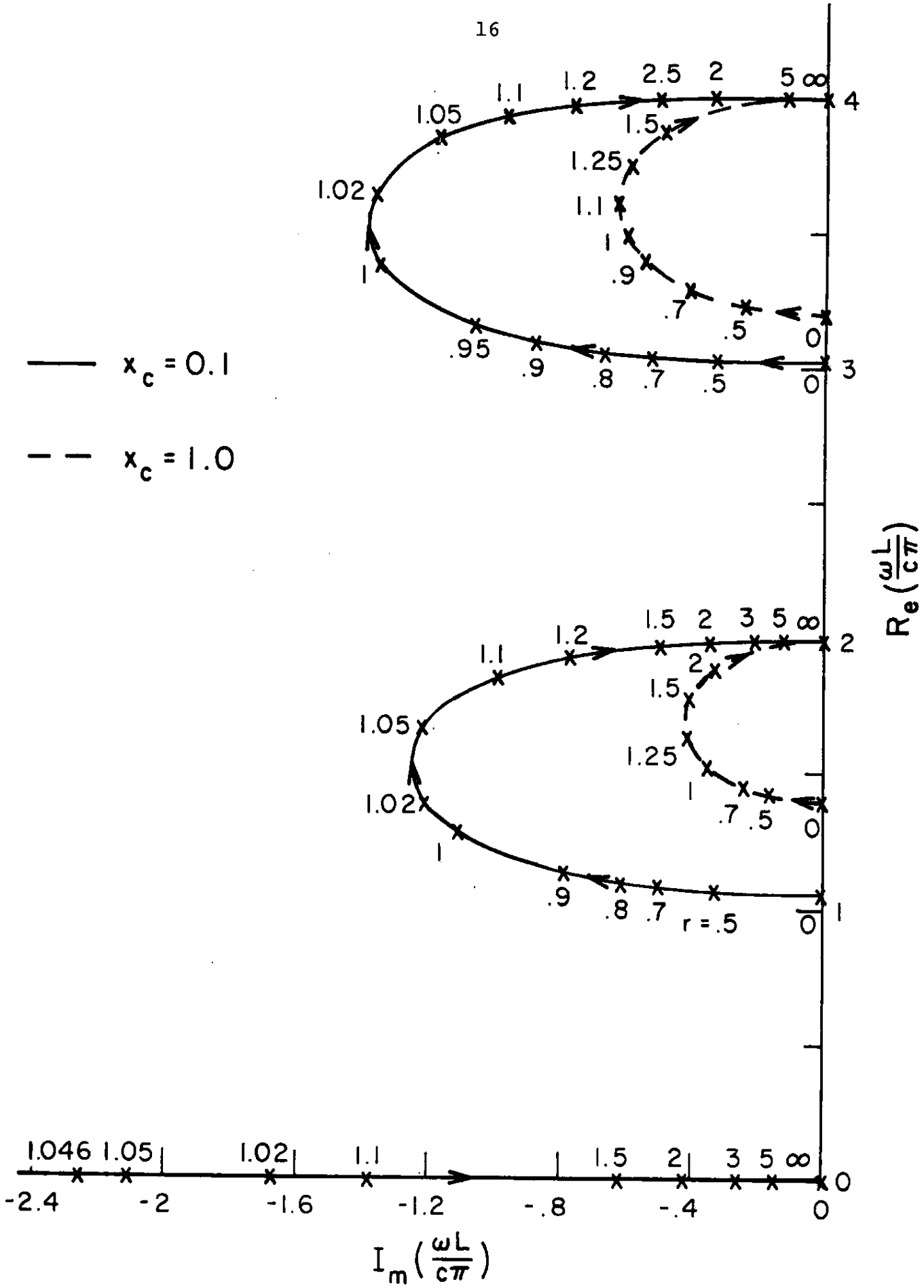

Fig. 4: Variation of the natural frequencies of a series $R_\ell - C_\ell$ center-loaded transmission line as a function of $r = R_\ell/R_0$; $Z_\ell = R_0(r + \frac{i}{S}x_c)$, $S = \omega L/c\pi$, $x_c = 0.1$ and 1.

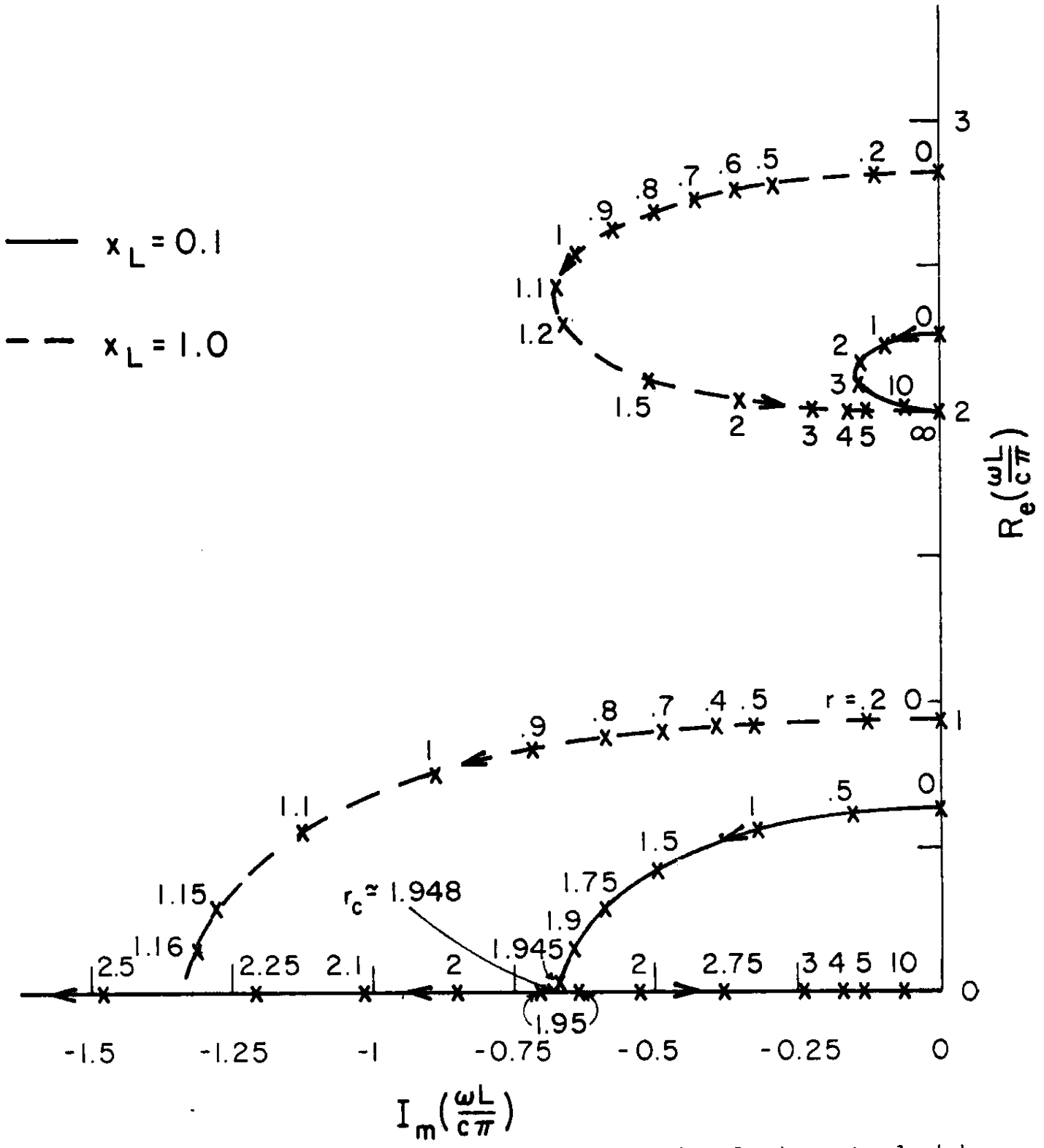

Fig. 5: Variation of the natural frequencies of a series $R_\ell - L_\ell$ center-loaded transmission line as a function of $r = R_\ell/R_0$; $Z_\ell = R_0(r - iSx_L)$, $S = \omega L/c\pi$, $x_L = 0.1$ and 1.

for a line with arbitrary-located load, and

$$[\Gamma_t(\omega_c^\ell)\ \Gamma_\ell(\omega_c^\ell)]' + i\,\frac{L}{c}\,\Gamma_t(\omega_c^\ell)\ \Gamma_\ell(\omega_c^\ell) = 0 \tag{35}$$

for a center-loaded symmetric-terminated line. Equation (34) or (35) can be used together with equation (22) or (28.2) to determine ω_c^ℓ and its corresponding r_c. By an analogy to circuit theory [12] a loaded line which satisfies the condition in (34) or (35) may be called a "critically-damped" transmission line. For the examples in Fig. 5 the line is "critically-damped" at $r_c \simeq 1.164$, for $x_L = 0.1$, and at $r_c \simeq 1.948$, for $x_L = 1$.

c) Resistive load in parallel with a capacitance ($R_\ell \parallel C_\ell$):

In Fig. 6 the natural frequencies of a parallel $R_\ell \parallel C_\ell$ loaded line for $x_c = 10$ and 100, with r varies from 0 to ∞ are depicted. The results resemble those of the series $R_\ell - C_\ell$ case in Fig. 4 with two important differences. First the zero order (i.e., "evanescent") mode for $R_\ell \parallel C_\ell$ load in Fig. 6 exists for $0 \le r < \infty$, while for $R_\ell - C_\ell$ loaded line, this mode exists only when $r \ge 1$. Secondly, as order of the modes increases, $\mathrm{Im}(\omega_s^\ell)$ of the "turning" points (i.e., points where $|\mathrm{Im}(\omega_s^\ell)|$ is maximum), for $R_\ell \parallel C_\ell$ loaded line decreases while for $R_\ell - C_\ell$ case increases. It is worthy to mention that this latter behavior of the parallel $R_\ell \parallel C_\ell$ loaded transmission line is similar to that of the natural frequencies of a resistively center-loaded thin-wire cylindrical antenna [7]. It is not surprising then to find out that for the latter problem, gap width of a lumped resistive load can have a distinctive effect on natural frequencies, as noted in [7].

d) Resistive load in series with both a capacitance and an inductance ($R_\ell - L_\ell - C_\ell$):

Figure 7 shows the locations of the first three (even) natural frequencies of a series $R_\ell - L_\ell - C_\ell$ center-loaded transmission line in the complex ω-plane.

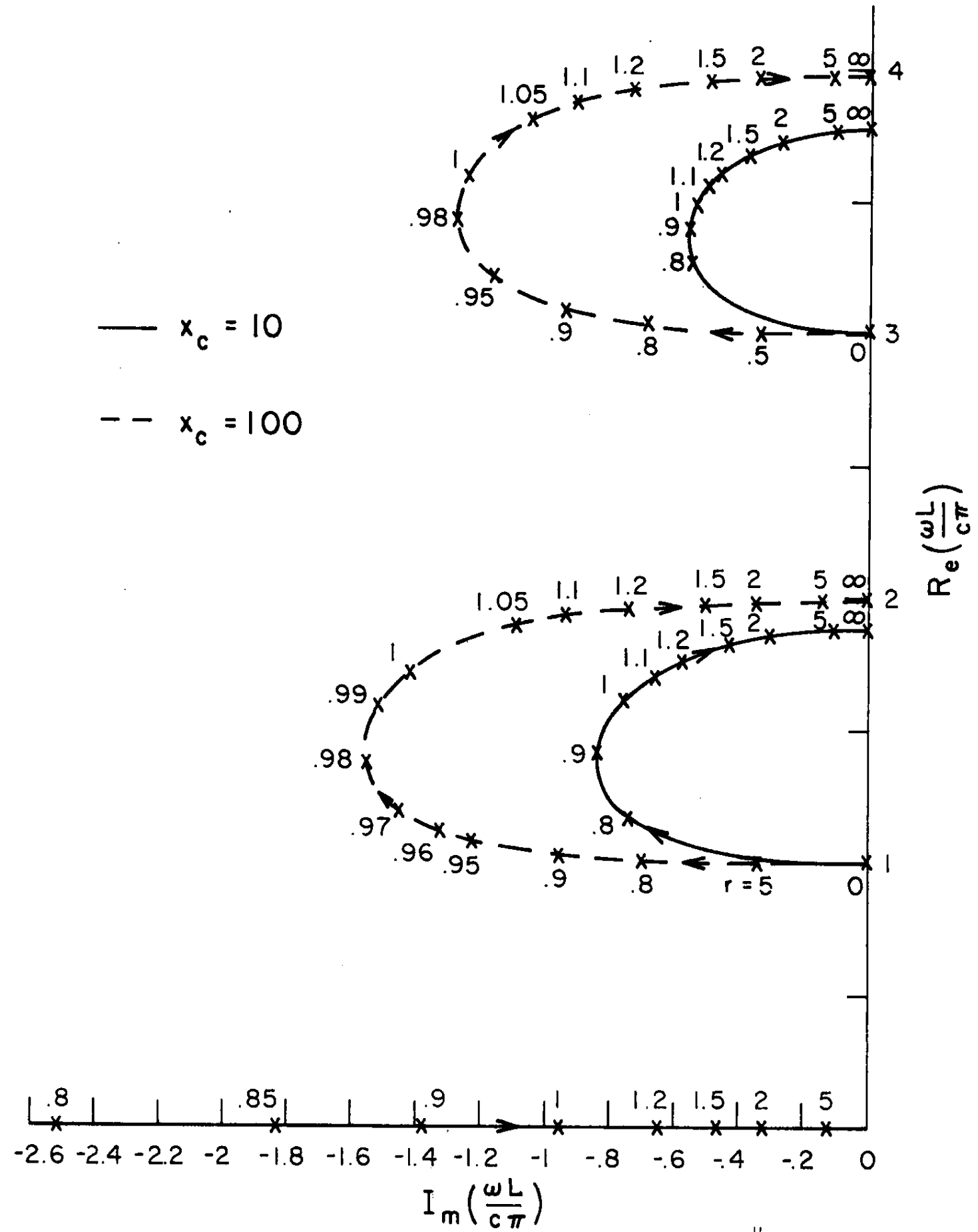

Fig. 6: Variation of the natural frequencies of a parallel $R_\ell \| C_\ell$ center-loaded transmission line as a function of $r = R_\ell/R_o$; $Z_\ell = R_o\left(\frac{r}{1 - iSr/x_c}\right)$, $S = \omega L/c\pi$, $x_c = 10$ and 100.

The results are plotted for $x_c = 0.1$ and various values of the inductive impedance x_L. In general, one can conclude from the behavior of the natural frequencies in Fig. 7 that adding a very small inductance x_L to the $R_\ell - C_\ell$ load of Fig. 4, causes a particular (2s-1)th mode to approach the negative imaginary axis, as r increases, and form a double pole there with $-\omega_s^{\ell *}$ at $r_c = 1 + \varepsilon (\varepsilon << 1)$; while the rest of the modes, (2s - 3)th and lower, traverse in a similar fashion as a $R_\ell - C_\ell$ loaded case. For this particular pair however, the double pole splits into two poles moving away from each other along the negative imaginary axis when $r > 1 + \varepsilon$, reminiscent of a $R_\ell - L_\ell$ circuit. Now, by slightly increasing x_L, for some value of r, the degeneracy between the (2s-1)th and (2s-3)th modes occurs; and then the (2s-1)th mode approaches $(\frac{L}{c\pi})\omega^{\ell}_{2s-2} = 2s-2$ (note that the odd modes $(\frac{L}{c\pi})\omega_{2s} = 2s$, $s = 0,1,2,\ldots$ remain unaffected by the center-load) and (2s-3)th mode shifts down toward the imaginary axis. By increasing x_L this process continues; as can be seen in Fig. 7 for $x_L = 0.01$, fifth natural frequencies shift down toward $(\frac{L}{c\pi})\omega_4 = 4$ as r varies from 0 to ∞, while third one approaches the negative imaginary axis to form the double pole and then split into two modes. Meanwhile for $x_L = 0.01$, the first natural frequency shifts up toward $(\frac{L}{c\pi})\omega_2 = 2$ as $r \to \infty$ and behaves like that of a R_ℓ-C_ℓ loaded line in Fig. 4. By increasing x_L, for some certain values of r and x_L, $0.01 < x_L < 0.1$, the degeneracy between the third and first modes occurs, and finally for $x_L \geq 0.1$ all of the modes behave like those in Fig. 5. for the $R_\ell - L_\ell$ loaded line. It may be useful to mention that the degenerate modes in the complex ω-plane as well as the double mode on the imaginary axis satisfy the equation (35).

Based on the above explanation for the behavior of the natural frequencies of a $R_\ell - L_\ell - C_\ell$ loaded line, one may now argue that for the $R_\ell - C_\ell$ load

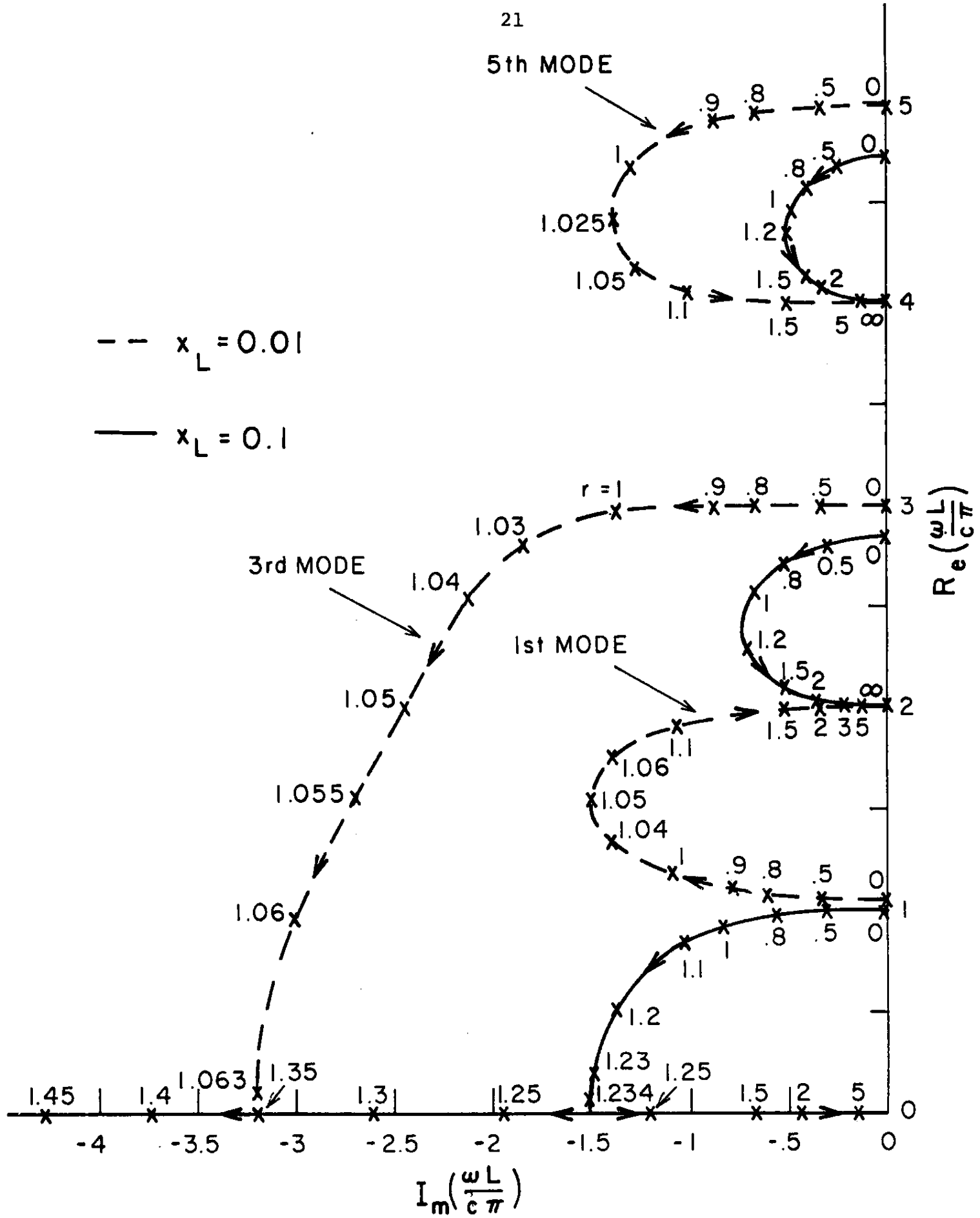

Fig. 7: Variation of the natural frequencies of a series $R_\ell - L_\ell - C_\ell$ center-loaded transmission line as a function of $r = R_\ell/R_o$; $Z_\ell = R_o(r - iSx_L + i/S\, x_c)$, $S = \omega L/c\pi$, $x_c = 0.1$, $x_L = 0.01$ and 0.1.

in Fig. 4, the natural frequency at $-i\infty$ on the imaginary axis, as r approaches 1, is a <u>double</u> pole which is formed by the (even) ∞-th mode and its conjugate pair, $-\omega_{\infty}^{\ell *}$, !. In fact $\omega_c^{\ell} = -i\infty$ at $r_c = 1$ for a R_ℓ - C_ℓ loaded line (which can be considered as a limiting case of a R_ℓ - L_ℓ - C_ℓ as $X_L \to 0$) satisfies the "critical-damping" condition in (35). Therefore, the "evanescent" natural frequencies on the imaginary axis for $r > 1$ in Fig. 4 are indeed the continuation of the locus of the ∞-th natural frequency in the complex ω-plane, as r varies from 1 to ∞.

In Fig. 8, we have shown the first two (even) natural frequencies of a $(R_\ell - L_\ell) \,||\, C_\ell$ center-loaded transmission line, for $x_L = 0.075$, $x_c = 10$, and as r varies from 0 to ∞. Although it is not shown in Fig. 8, but we found the natural frequencies of this line to behave like those of the series R_ℓ - L_ℓ - C_ℓ case in Fig. 7, as x_L varies. For the latter case however, the double pole (i.e., "critical-damping") always occurs for a "critical" load $r_c > 1$, whereas for the $(R_\ell - L_\ell) \,||\, C_\ell$ case in Fig. 8, we have $r_c > 1$; this is expected because of the behavior of the natural frequencies of the $R_\ell || C_\ell$ loaded line in Fig. 6.

Before concluding the results for the center-loaded line, it is worthy to mention that simple approximate expressions for the "evanescent" natural frequencies (i.e., $\frac{\omega_o^{\ell} L}{c\pi} = -i\sigma_o$) can easily be obtained from (27.2). These approximations are given by

$$\sigma_o \simeq \frac{x_c}{r-1} \quad ; \qquad x_c >> r-1$$

for the R_ℓ - C_ℓ load,

$$\sigma_o \simeq (\frac{1-r}{r})x_c \quad ; \qquad \frac{1-r}{r} >> \frac{1}{x_c}$$

for the $R_\ell \,||\, C_\ell$ load, and

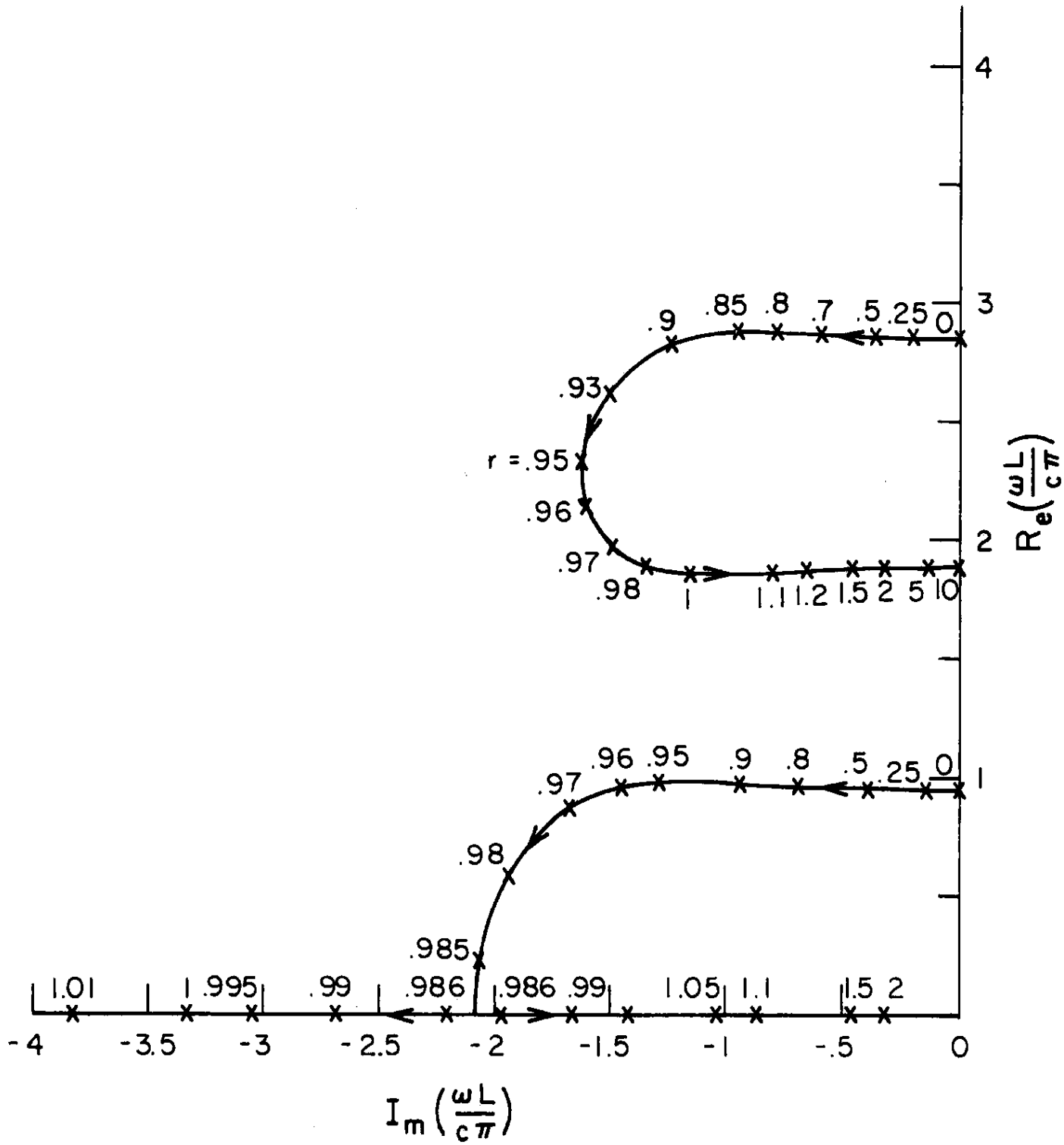

Fig. 8: Variation of the natural frequencies of a $(R_\ell\text{-}L_\ell)||C_\ell$ center-loaded transmission line as a function of $r = R_\ell/R_o$; $Z_\ell = R_o[(r - iSx_L)/(1 - S^2 x_L/x_c - iS\, r/x_c)]$, $S = \omega L/c\pi$, $x_c = 10$ and $x_L = 0.075$.

$$\sigma_{o2} \simeq \frac{r-1}{x_L} \quad ; \qquad r - 1 >> x_L$$

for the R_ℓ - L_ℓ load, where σ_{o2} corresponds to the second evanescent mode, i.e. the one with the larger σ_o.

Natural frequencies of an off-center loaded transmission-line

The natural frequencies of an off-center loaded transmission line are shown in Figures 9 and 10 for resistive and series R-C loads, respectively. In general for an off-center loaded line, there are <u>two</u> different sets of natural frequencies, each corresponding to resonances predominantly in one of the two segments of the transmission line, separated by the load.

a) Purely resistive load, i.e. $Z_\ell = R_\ell$

For a pure resistive load located at z = d, one set of natural frequencies vary from $\frac{L}{c\pi}\omega_s^\ell = 2s-1$, when r = 0, to $\frac{L}{c\pi}\omega_s^\ell = (\frac{L}{d})s$, s = 0,1,2,3,..., when r = ∞; whereas the other set vary from $\frac{L}{c\pi}\omega_s^\ell = 2s$, when r = 0, to $\frac{L}{c\pi}\omega_s^\ell = (\frac{1}{1 - d/L})\, s$, s = 1,2,3,..., when r = ∞. These two sets correspond to resonances which are predominant in the segments, 0 to d. and d to L of the line, respectively. In addition, it can be shown from eq. (29) that as $\frac{Z_\ell}{R_o} = r$ approaches 1, the first set of the natural frequencies behave like

$$\begin{cases} (\frac{L}{c\pi})\,\omega_s^\ell \simeq (\frac{L}{2d})[2s-1 - \frac{i}{\pi}\,\ell n\,(\frac{r}{1-r})], & r = 1 - \varepsilon \qquad (36.1) \\ (\frac{L}{c})\,\omega_s^\ell \simeq (\frac{L}{2d})[2s - \frac{i}{\pi}\,\ell n\,(\frac{r}{r-1})], & r = 1 + \varepsilon \qquad (36.2) \end{cases}$$

where s = 0, ±1, ±2,... and $\varepsilon << 1$. As shown in Figure 9, when the resistive load is located at $\frac{d}{L} = 0.35$ and as r increases, the first natural frequency shifts up in the complex ω-plane and behaves like (36.1) as r approaches 1. Meanwhile, the second natural frequency shifts down and approaches $\frac{1}{0.65}$ on the real axis, as r varies from 0 to ∞.

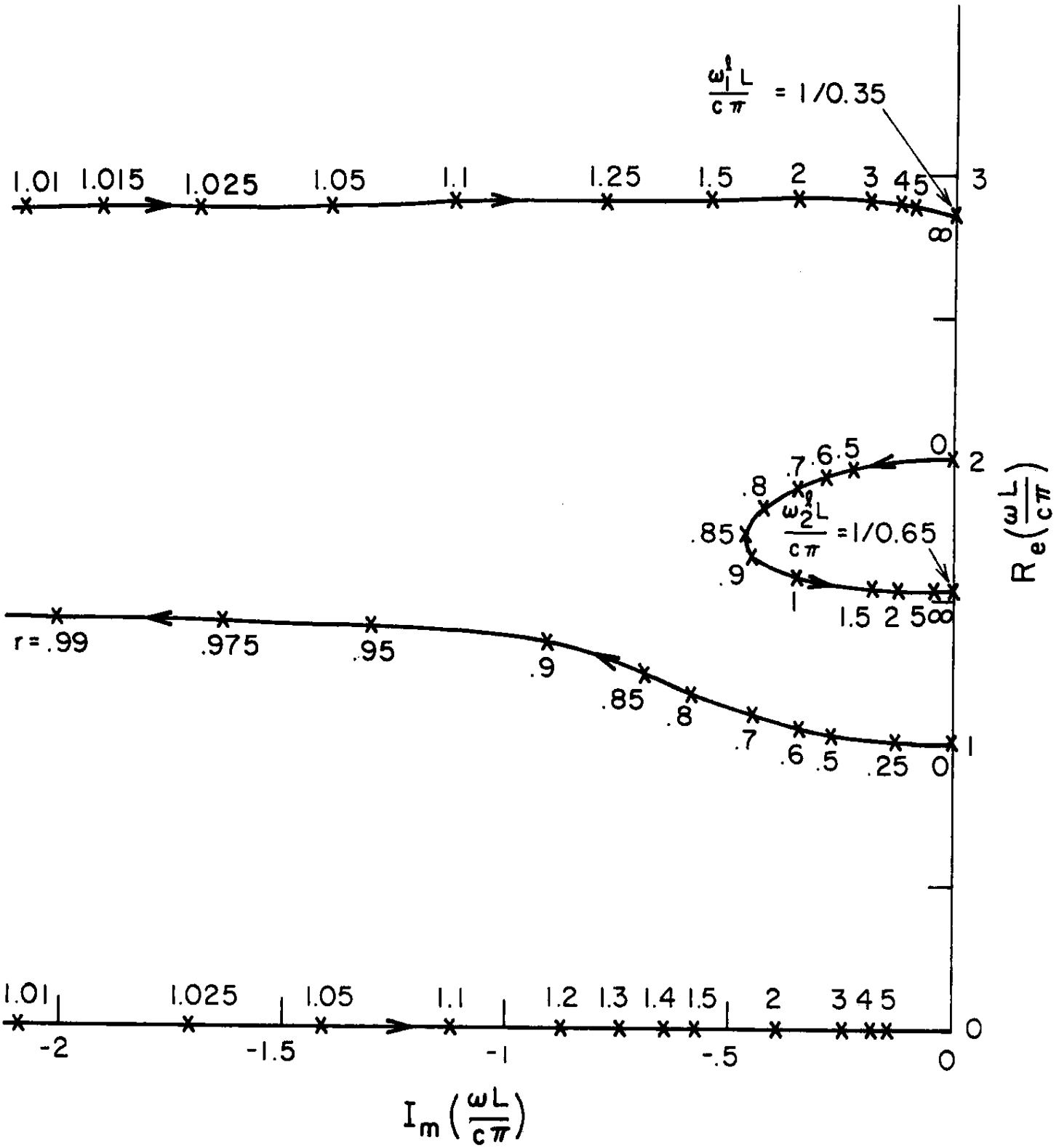

Fig. 9: Variation of the natural frequencies of a resistively off-center ($\frac{d}{L}$ = 0.35) loaded transmission line as a function of $r = r_\ell/R_o$.

b) Resistive load in series with a capacitance, $R_\ell - C_\ell$

Figure 10 shows the behavior of the natural frequencies in the complex ω-plane when a capacitance is added to the resistive load of Fig. 9. As shown in Fig. 10, for the capacitive impedance $x_c = 0.05$ and as the values of the resistor r increases from 0 to ∞, the natural frequencies of the first two modes move transversely in opposite directions, while those of the higher order modes move in the same direction, upward, in the complex ω-plane. By increasing x_c however, for some specific values of r and x_c, $0.05 < x_c < 0.1$, the first two modes become degenerate, i.e. $\omega_1^\ell = \omega_2^\ell$, and finally as shown in the figure, for $x_c = 0.1$, the first and second natural frequencies shift up in the complex ω-plane and approach the points $\frac{1}{0.65}$ and $\frac{1}{0.35}$ on the real axis, respectively, as r approaches infinity. As will be shown later, for $x_c = 0.1$ the first and second natural frequencies correspond to resonances predominantly in the two segments, $z = 0.35\,L$ to L, and $z = 0$ to $0.35\,L$, of the loaded line. As can be seen in Fig. 10, there is also an "evanescent" mode with natural frequencies located on the negative imaginary axis (shown only for $x_c = 0.1$ case). As was discussed earlier for the center-loaded line, these natural frequencies can be interpreted as those of the ∞-th mode for $r \geq 1$.

Although it is not shown in Figure 10, but it is evident that for some values of r and $x_c < 0.05$, the degeneracy between the higher order modes of the two sets of natural frequencies can occur. In fact, adding an infinitesimal capacitance to the resistive load of Fig. 9 causes all of the natural frequencies of the two set shift transversely in the opposite directions in the complex ω-plane, as r increases from 0 to ∞. By increasing the values of the capacitive impedance x_c, the modal degeneracies occur

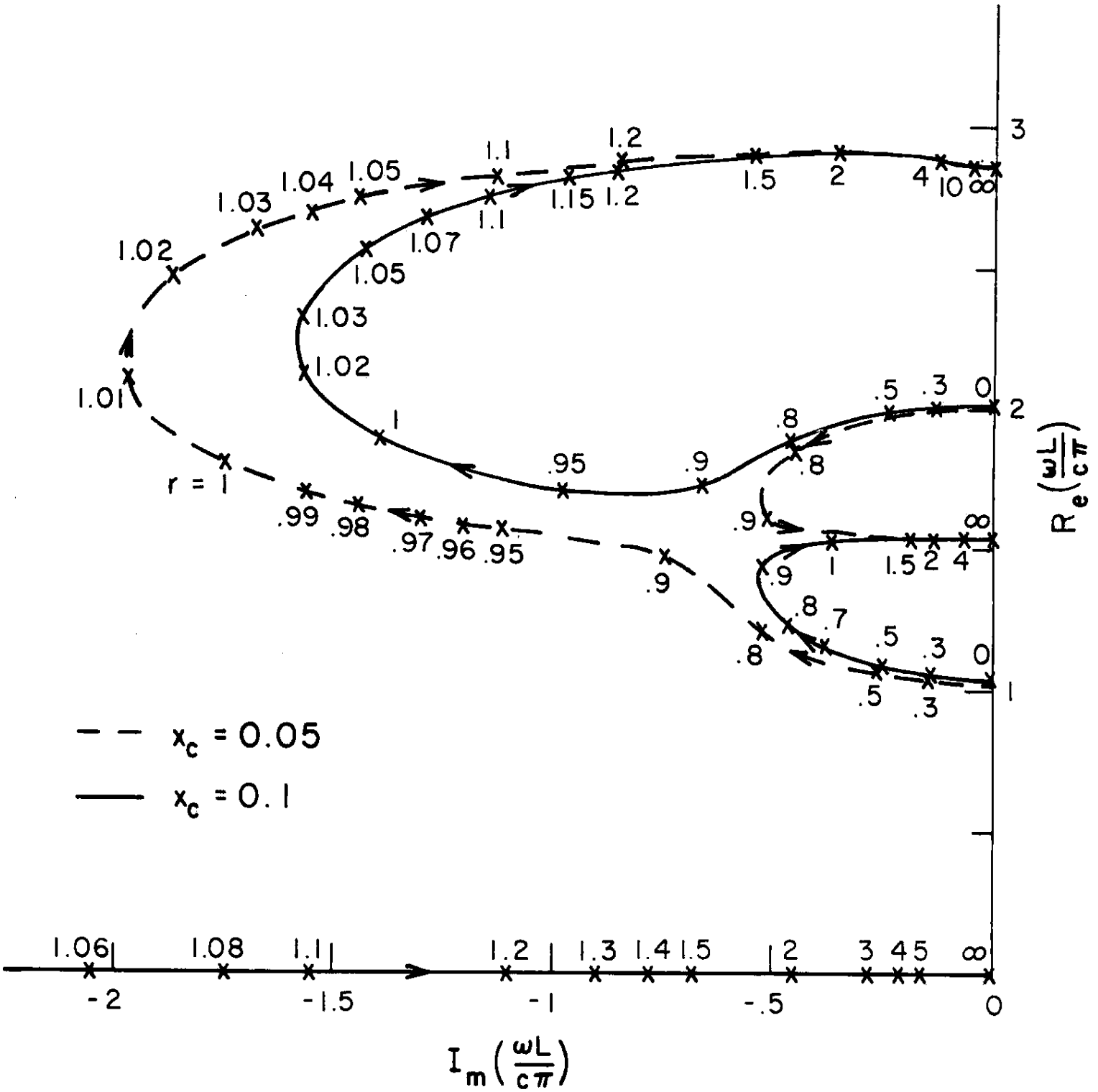

Fig. 10: Variation of the natural frequencies of a series R_ℓ - C_ℓ off-center ($\frac{d}{L}$ = 0.35) loaded transmission line as a function of $r = R_\ell/R_o$; $Z_\ell = R_o(r + \frac{i}{S} x_c)$, $S = \omega L/c\pi$, x_c = 0.05 and 0.1.

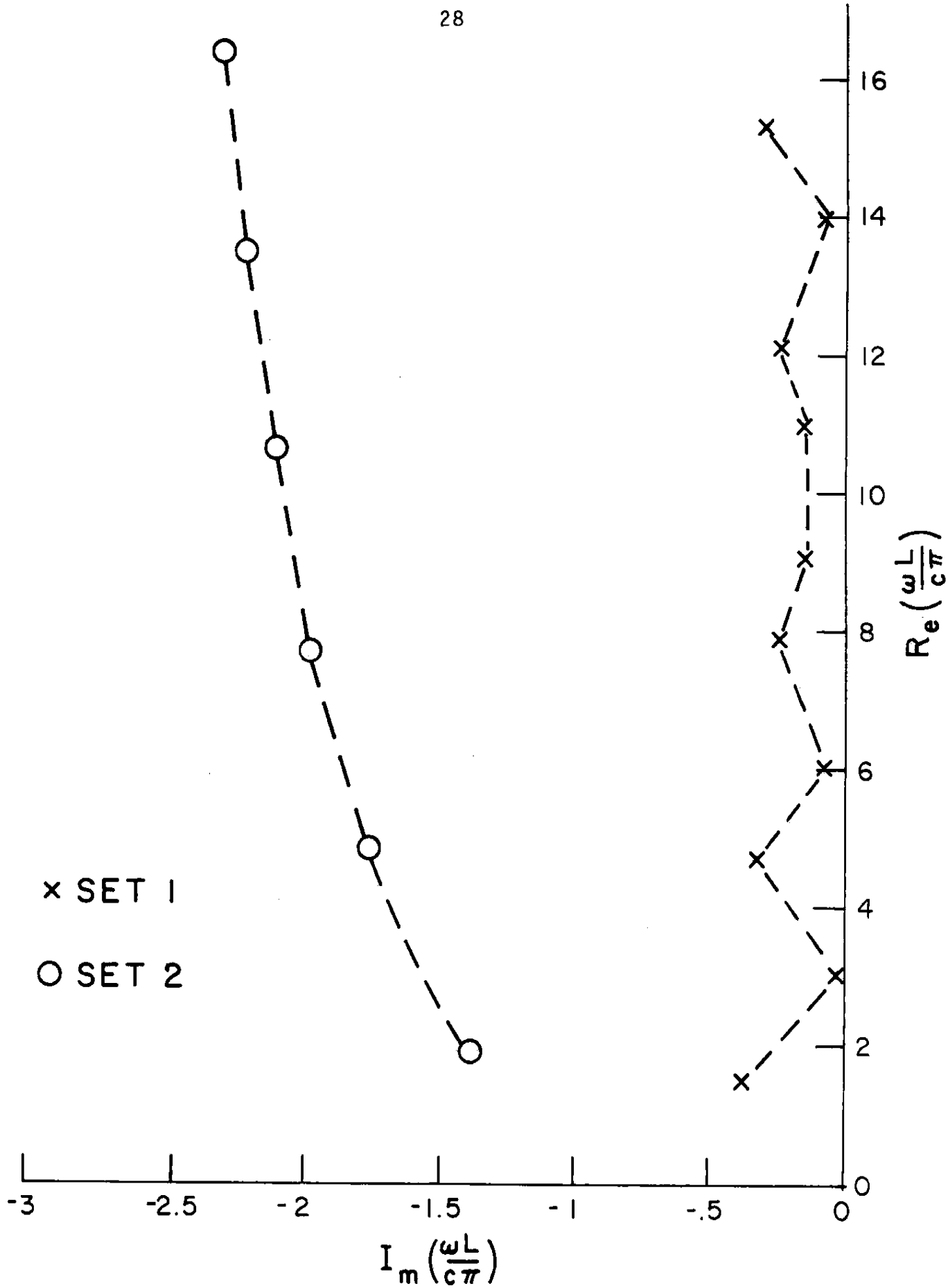

Fig. 11: The two sets of natural frequencies for a transmission line with an off-center $R_\ell - C_\ell$ load located at d/L = 0.35; r = 1, and $x_c = 0.1$.

and finally as was discussed earlier, for $x_c \geq 0.1$ all of the natural frequencies of the two sets move in the same direction, i.e., upward, in the ω-plane, as r varies between 0 and ∞.

Finally, the first ten natural frequencies of the two sets of modes, for $x_c = 0.1$ and $r = 1$, are shown in Fig. 11. As can be seen, one set has a much larger $|I_m(\omega_s^{\ell})|$ than the other one; hence a more rapid decay in time of modes of the former set is expected.

3.1.3 Current distributions of the natural modes

Normalized current distributions of the lower order natural modes of $R_\ell - C_\ell$ and $R_\ell - L_\ell$ loaded, open-circuit transmission lines are discussed in this section. For an open circuit terminated line, the natural mode distribution is given by $F_s(z)$ in (30). The results presented here however, are normalized such that for each mode $F_s(z)$ has a maximum magnitude of one.

a) Natural modes distributions of a center-loaded transmission line.

Figures 12-a and 12-b show the (magnitude) distribution of the first natural mode for a $R_\ell - C_\ell$ center-loaded line with $x_c = 0.1$. As shown in the figures, the current distribution of the first natural frequency varies from a symmetric mode, given approximately by $\sin(\pi z/L)$, when $r = 0$, to a mode given by $|\sin(2\pi z/L)|$, when $r = \infty$. Near the "turning" point region, $r \simeq 1$, the mode has nearly a hyperbolic-sine, sinh, distribution. We note that in this region the time domain response of such a mode decays rapidly because of the large value of its $I_m(\omega_1^{\ell})$ in Fig. 4.

Figures 13-a and 13-b show the first natural mode current distribution of an $R_\ell - L_\ell$ center-loaded line, for a normalized inductive impedance $x_L = 1.0$. One can see in these figures that as r approaches the "critical" value of

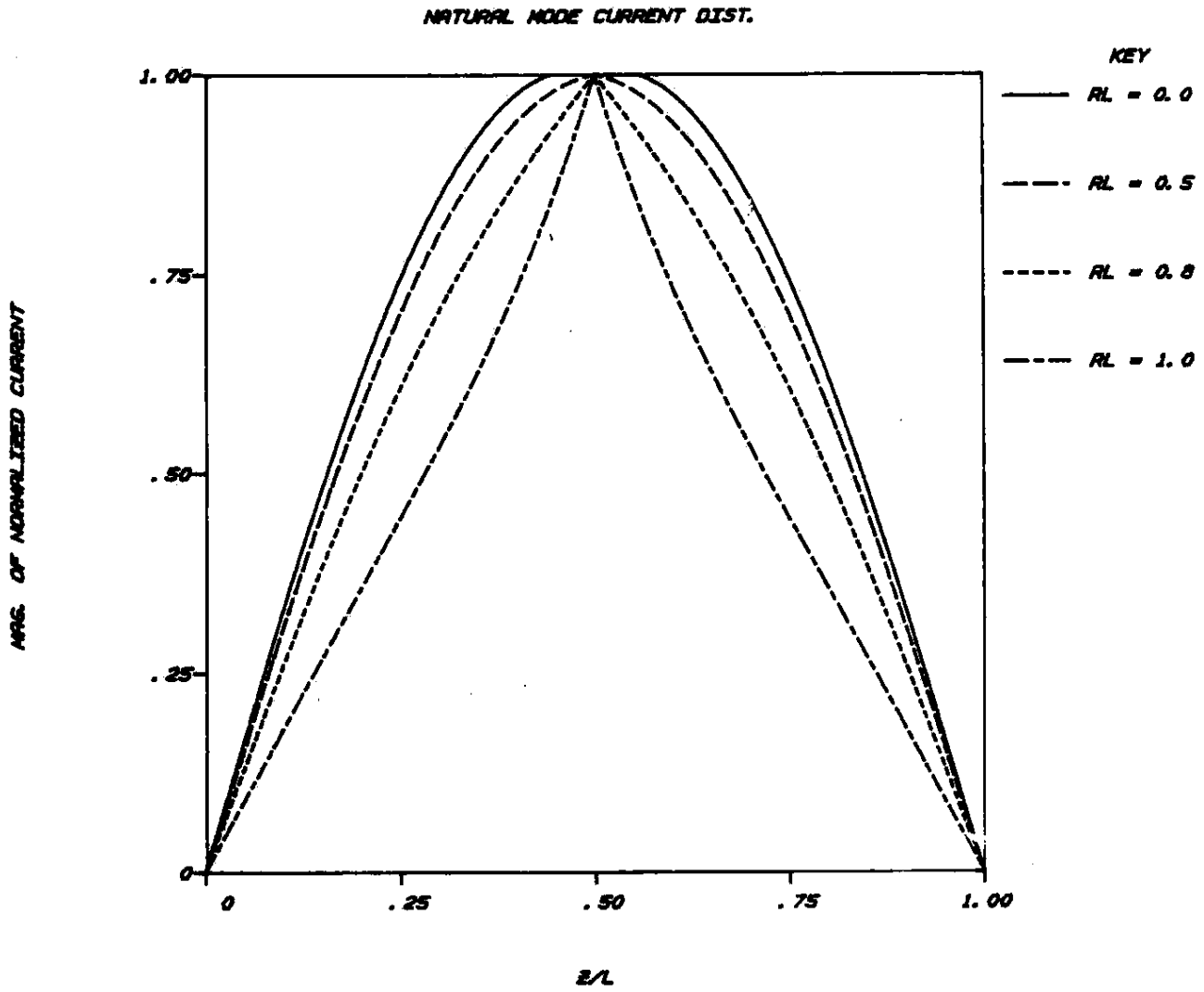

Fig. 12-a: First normalized natural mode current distribution of a series $R_\ell - C_\ell$ center-loaded transmission line, for $x_c = 0.1$ and various values of $r = R_\ell/R_o \leq 1$.

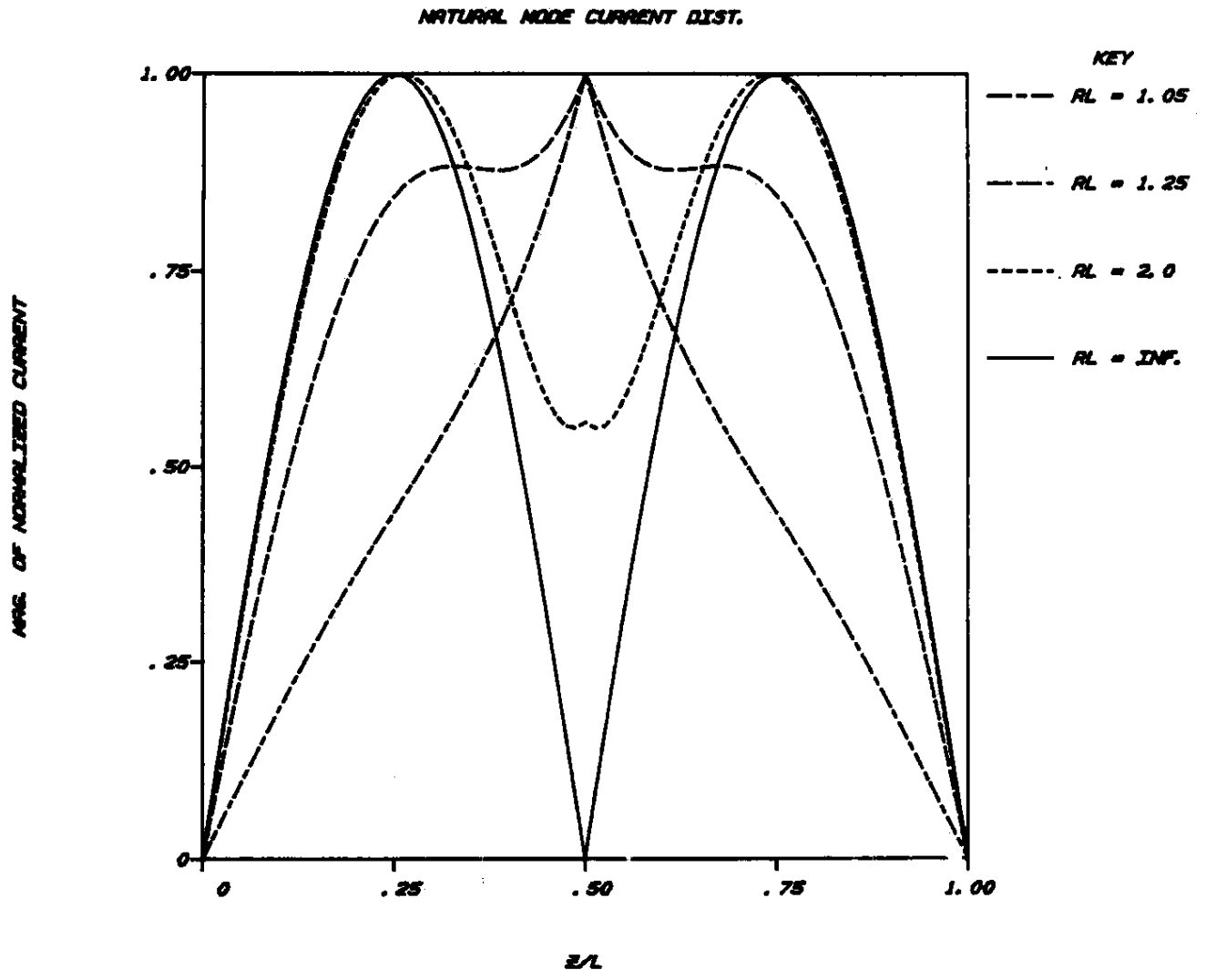

Fig. 12-b: First normalized natural mode current distribution of a series $R_\ell - C_\ell$ center-loaded transmission line, for $x_c = 0.1$ and various values of $r = R_\ell/R_o > 1$.

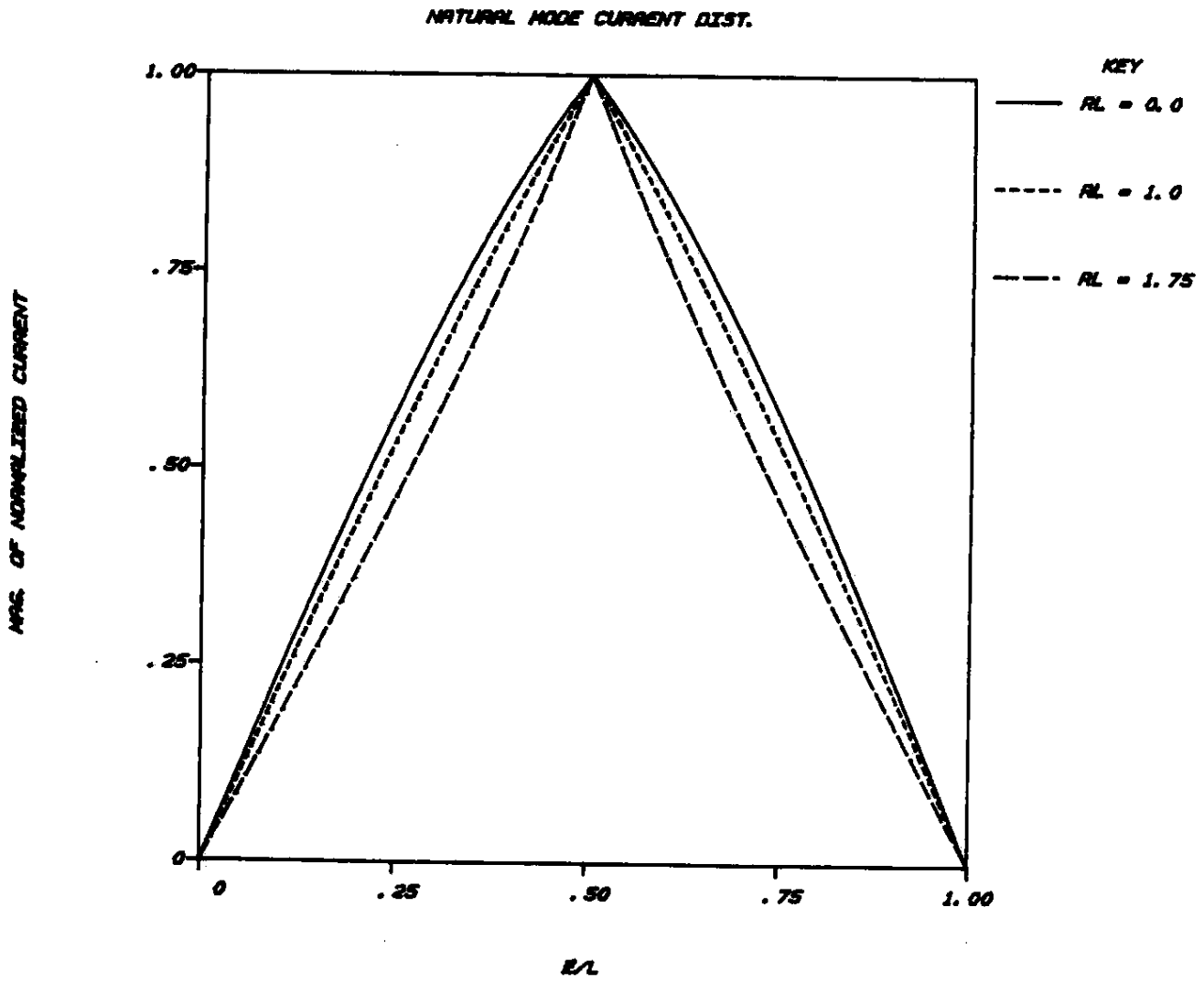

Fig. 13-a: First normalized natural mode current distribution of a series $R_\ell - L_\ell$ center-loaded transmission line, with $x_L = 1.0$ and for values of r smaller than the "critical" resistor, $r_c \simeq 1.948$.

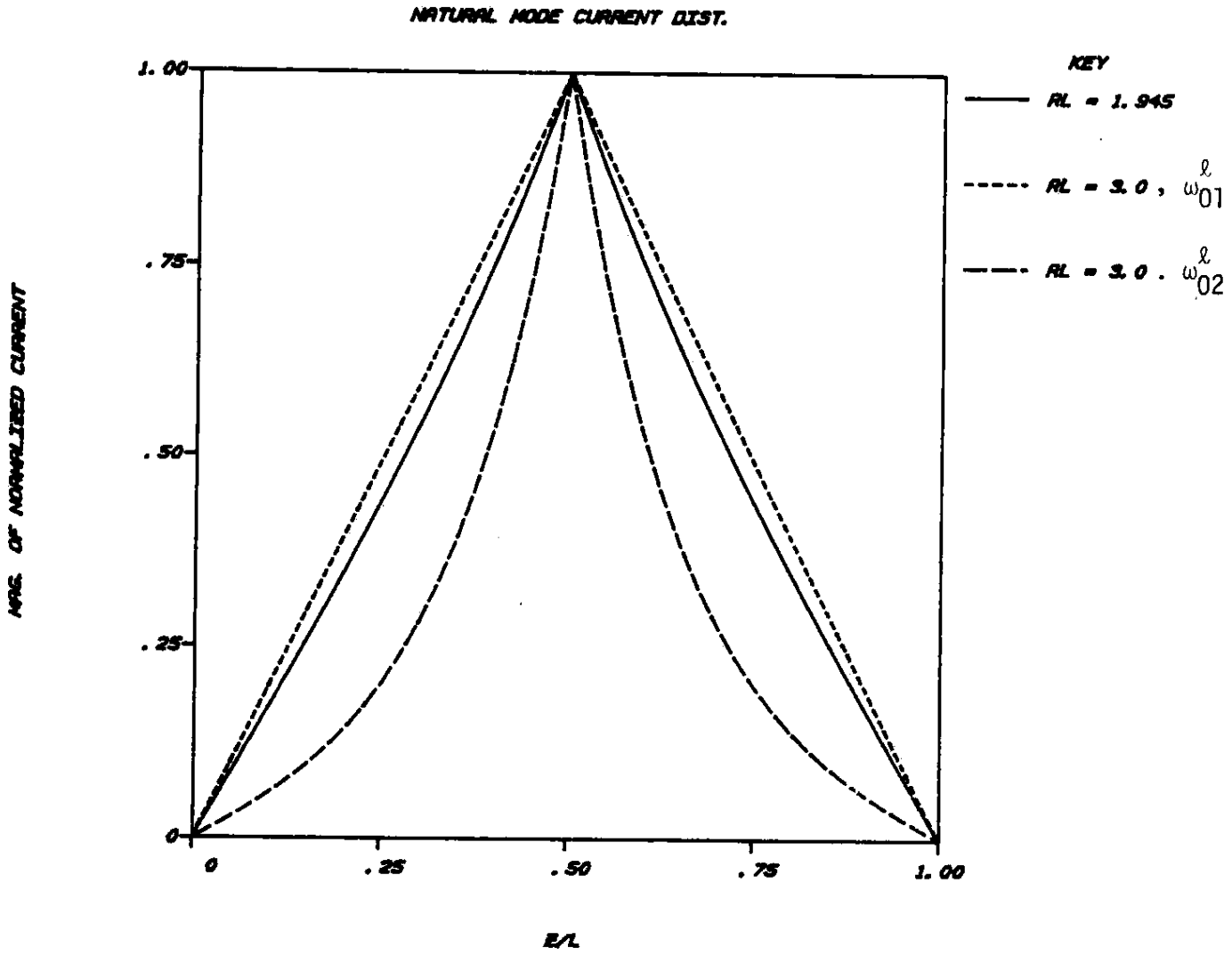

Fig. 13-b: First normalized natural mode current distribution of a series R_ℓ-L_ℓ center-loaded transmission line for $x_L = 1.0$ and various values of $r = R_\ell/R_o$. For $r > r_c$, the first mode splits into two "evanescent" modes; for $r = 3$, these modes correspond to the natural frequencies, $(L/c\pi)\omega_{01}^{\ell} = -i0.23166$ and $(L/c\pi)\omega_{02}^{\ell} = -i1.9962$.

$r_c \simeq 1.948$ (corresponding to the double pole in Fig. 5) the mode distribution along the line approaches a sinh form. Then for $r \searrow r_c$, as shown in Fig. 13-b, the first natural mode splits apart into the two modes both having an entirely sinh distribution. In time-domain however, one of the modes, i.e. ω_{02}^{ℓ}, is expected to decay faster than the other one, due to the larger attenuation of its natural frequency in Fig. 5.

b) Natural modes distributions of an off-center loaded-transmission line.

In order to investigate the effect of an off-set, normalized natural mode current distributions of a transmissin line with an off-center load, $R_\ell - C_\ell$, located at $\frac{d}{L} = 0.35$, are shown in Figs. 14-15. The results are plotted for the normalized capacitive impedance $x_c = 0.1$. Figure 14 shows the current distribution of the first natural mode for such a line. As shown, this distribution varies from the symmetric mode of a line of length L, when $r = 0$, to the one corresponding to a line of length 0.65 L, when $r = \infty$. For the second mode in Figs. 15-a and 15-b however, the current distribution varies from the unsymmetric mode of a line of length L, when $r = 0$, to the one corresponding to a line of length 0.35 L, when $r = \infty$. In addition, it can now be clearly seen from Figs. 14-15 that the first and second modes resonate predominantly in the two segments, 0.35L to L, and 0 to 0.35L, of the transmission line, respectively; confirming our earlier discussion, regarding the existence of these two different sets of natural modes on an off-center loaded-line. These two sets of natural mode complement each other's distribution along the line for $r \gg 1$ as shown in Figs. 14 and 15-b for $R_\ell - C_\ell$ load as r approaches ∞, and as can clearly be seen in Fig. 16 for a resistive-loaded line. In the latter case, resistive load with the normalized value of $r = 5$

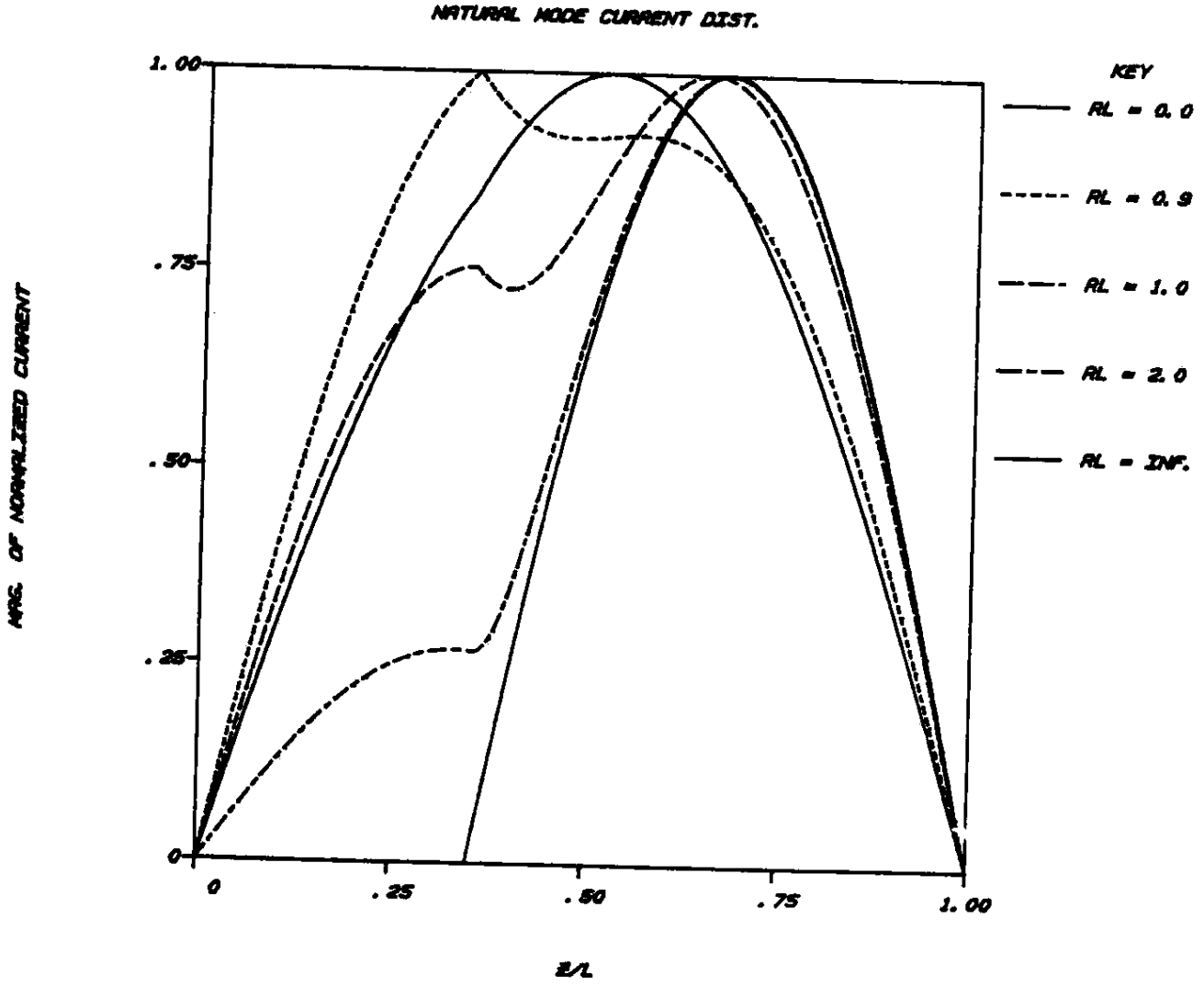

Fig. 14: First normalized natural mode current distribution of a series $R_\ell - C_\ell$ off-center loaded transmission line with d/L = 0.35, x_c = 0.1 and as the value of $r = R_\ell/R_o$ varies from zero to infinity.

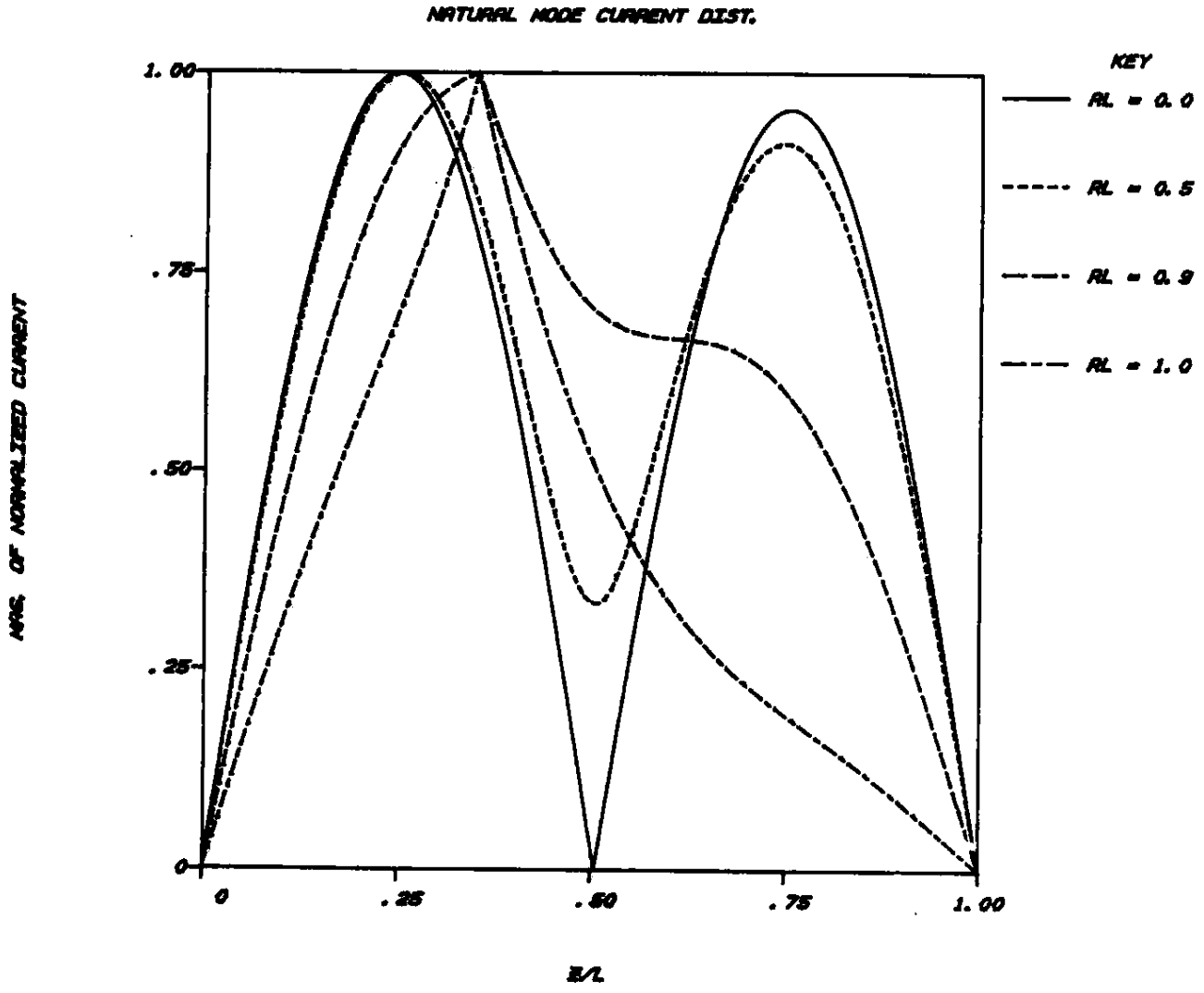

Fig. 15-a: Second normalized natural mode current distribution of a series $R_\ell - C_\ell$ off-center loaded transmission line with $d/L = 0.35$, $x_c = 0.1$ and for various values of $r = R_\ell/R_o \leq 1$.

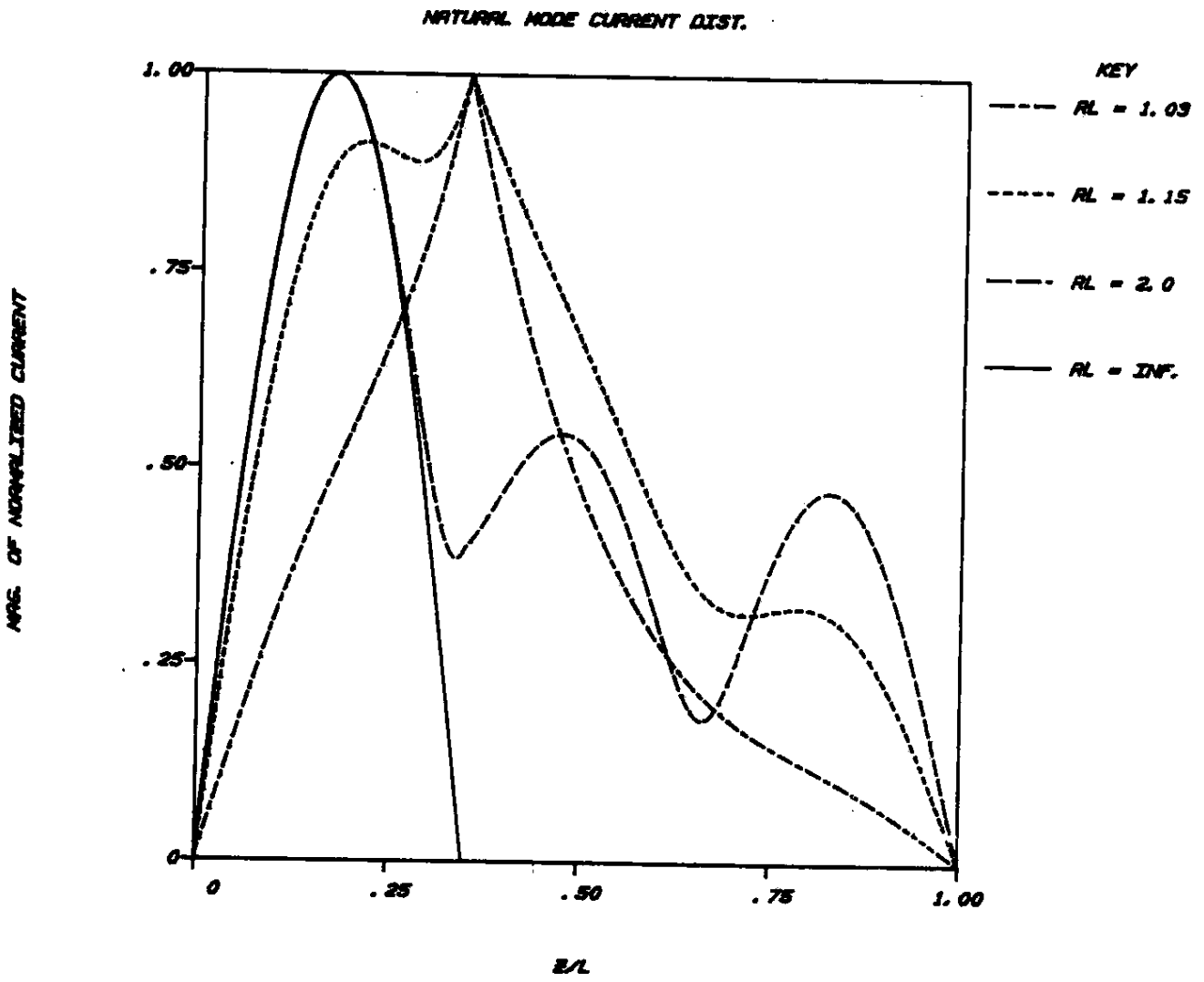

Fig. 15-b: Second normalized natural mode current distribution of a series $R_\ell - C_\ell$ off-center loaded transmission line with d/L = 0.35, x_c = 0.1 and for various values of $r = R_\ell/R_0 > 1$.

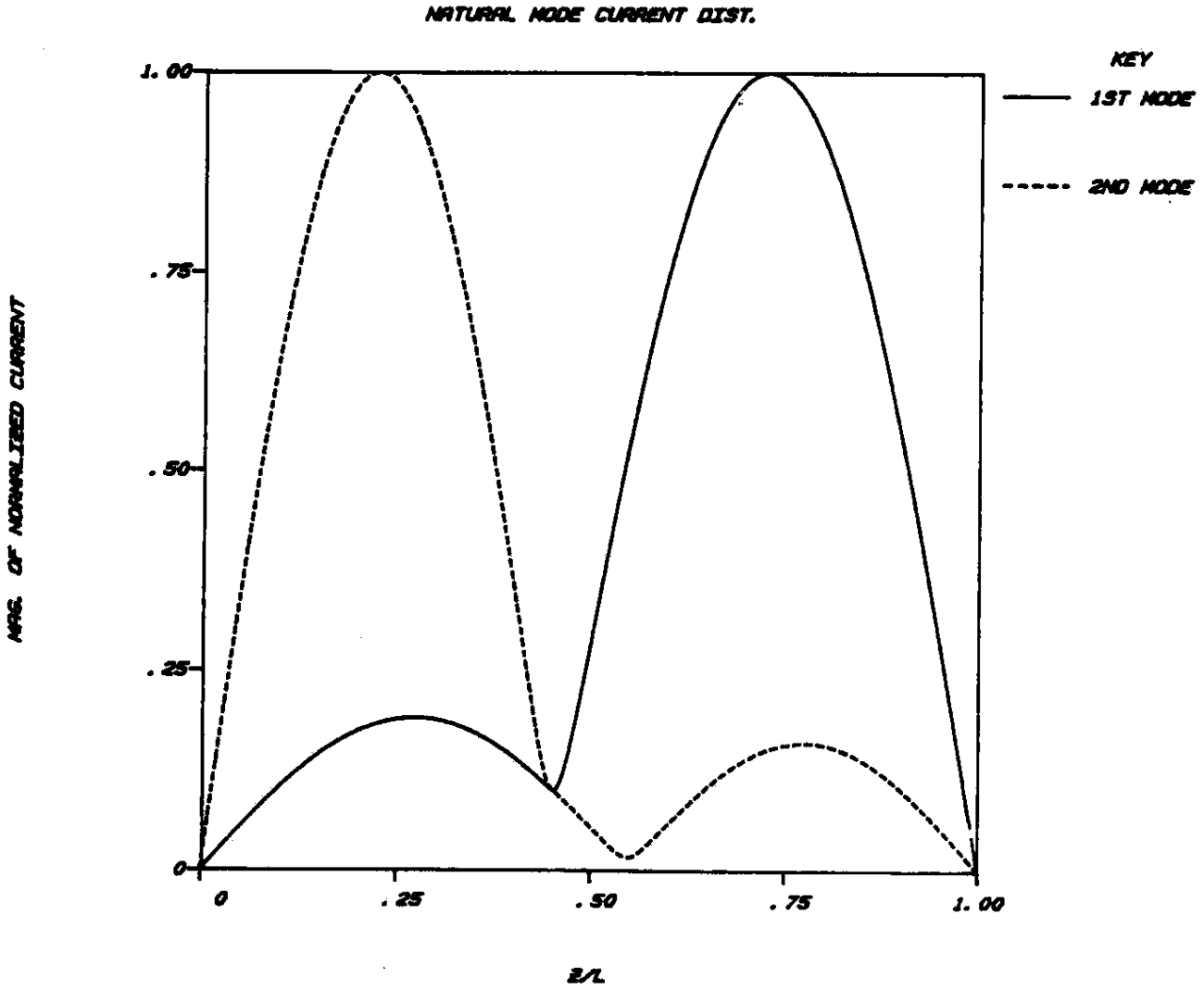

Fig. 16: First and second normalized natural mode current distributions for a transmission line with an off-center resistive load r = 5, located at d/L = 0.45.

is located at $\frac{d}{L} = 0.45$, and the corresponding results are plotted for the first two natural frequencies, $\frac{L}{c\pi}\omega_1^{\ell} = 1.82763 - i0.058265$ and $\frac{L}{c\pi}\omega_2^{\ell} = 2.21336 - i0.072131$. As shown in Fig. 16, the normalized current distributions of ω_1^{ℓ} and ω_2^{ℓ} are predominantly resonant in the segments 0.45 to L and 0 to 0.45 L of the line, respectively. Finally, as can be seen in Figs. 14-15, the first and second natural modes, for the $R_{\ell} - C_{\ell}$ loaded line have nearly sinh distributions for $r \simeq 0.9$ and $1 \leq r \leq 1.03$, respectively. These distributions are expected because of the behavior of the natural frequencies in the complex ω-plane for these values of r, which are in the "turning point" regions as shown in Fig. 10.

It should be noted that the current distributions plotted in Figs. 12-16 were normalized and did not show the relative excitation of each mode. The problems of mode excitation is physically more relevant and meaningful when it is studied in the time-domain. This problem will be discussed in section 3.2.2.

3.2 Transient Response of a Loaded Transmission Line, Driven by a Pair of Slice Voltage Generators

3.2.1 The SEM Representation.

Let us suppose that the impedance loaded transmission line of Fig. 1-b is driven by a pair of slice voltage generators $\pm V_g(t)$, $V_g(t) = V_o H(t-t_o)$ located at $z = z'$. The total current distribution on the line can be obtained by superposition of the currents due to the real and "fictitious" sources located at z' and d, respectively. By using (5), we therefore have

$$\tilde{I}^{\ell}(\omega;z,z') = \tilde{V}_g(\omega)\ Y(\omega;z,z') + \tilde{V}_Z(\omega)\ Y(\omega;z,d) \qquad (37)$$

where $\tilde{V}_Z(\omega) = -Z_{\ell}(\omega)\ \tilde{I}^{\ell}(\omega;d,z')$ is the voltage developed across the load impedance $\tilde{Z}_{\ell}$; $\tilde{V}_g(\omega) = \frac{V_o e^{+i\omega t_o}}{i\omega}$ is the Fourier transformation of $V_g(t)$

and $Y(\omega;z,z')$ is given by (20). We may now solve (37) at $z = d$ to obtain $\tilde{I}^{\ell}(\omega;d,z')$,

$$\tilde{I}^{\ell}(\omega;d,z') = \frac{\tilde{V}_g(\omega)\Delta(\omega)}{D(\omega)} Y(\omega;d,z') \tag{38}$$

where $\Delta(\omega)$ and $D(\omega)$ are given by (9) and (23) respecitvely. Subsequently the total current in (37) can be written as

$$\tilde{I}^{\ell}(\omega;z,z') = \tilde{V}_g(\omega)[Y(\omega;z,z') - \frac{Z_{\ell}(\omega)\Delta(\omega)}{D(\omega)} Y(\omega;d,z') Y(\omega;z,d)] \tag{39.1}$$

$$= \frac{\tilde{V}_g(\omega)e^{-i\frac{\omega}{c}L}}{R_o\Delta(\omega)} \left[f(\omega;z,z') - \frac{Z_{\ell}(\omega)}{R_o} \frac{e^{-i\frac{\omega}{c}L}}{D(\omega)} f(\omega;d,z')f(\omega;z,d)\right] \tag{39.2}$$

where in writing (39.2), the definition in (20) has been used. We note that from (23),

$$\frac{Z_o(\omega)}{R_o} e^{-\frac{i\omega}{c}L} = \frac{1}{f(\omega;d,d)} [D(\omega) - \Delta(\omega)] \tag{40}$$

which upon insertion into (39.2), yields the following result:

$$\tilde{I}_{\ell}(\omega;z,z') = \tilde{I}_{\ell}^{(0)}(\omega;z,z') + \frac{\tilde{V}_g(\omega)}{R_o} e^{-i\frac{\omega}{c}L} \tilde{\zeta}(\omega;z,z') \tag{41}$$

where

$$\tilde{I}_{\ell}^{(0)}(\omega;z,z') = \frac{V_g(\omega)}{R_o} \frac{e^{-i\frac{\omega}{c}L}}{D(\omega)f(\omega;d,d)} f(\omega;d,z')f(\omega;z,d) \tag{42}$$

and

$$\tilde{\zeta}(\omega;z,z') = \frac{1}{\Delta(\omega)} [f(\omega;z,z') - \frac{1}{f(\omega;d,d)} f(\omega;d,z')f(\omega;z,d)] \tag{43}$$

To this end, one may now substitute for f from (21) into (43) and see that

$$\tilde{\zeta}(\omega;z,z') = 0 \qquad \text{for} \quad z_< \leq d \leq z_>$$

and therefore for the case when the observation point and voltage source are located in two different segments of the line separated by the load, the current distribution can be further reduced to

$$\tilde{I}_\ell(\omega;z,z') = \tilde{I}_\ell^{(0)}(\omega;z,z') \qquad ; \quad z_< \le d \le z_>$$

$$= \frac{\tilde{V}_g(\omega)}{R_o} \quad \frac{e^{-i\frac{\omega}{c}L}}{D(\omega)} \, g_1(\omega;L - z_<)g_2(\omega;z_>) \tag{44}$$

for $z_< \le d \le z_>$ where $z_{\gtrless} = \max_{\min}(z,z')$. As can be seen, in addition to the pole singularity of $\tilde{V}_g(\omega)$, the only other singularities of (44) in the complex ω-plane are the roots of $D(\omega) = 0$.

For other values of d, $z_<$ and $z_>$ we note that:

i) $\tilde{\zeta}$ does not have any singularities at $\Delta(\omega) = 0$, as can be shown by using (21) and (43).

ii) $\tilde{I}_\ell$ does not possess any new pole at $f(\omega;d,d) = 0$, as can be shown from (41) and is apparent from (39).

Consequently, $\tilde{I}_\ell$ in (41) possesses pole singularities only at $D(\omega_s^\ell) = 0$, which appear in the first term (i.e., $\tilde{I}_\ell^{(0)}$) of (41). And therefore the expression for $\tilde{I}_\ell^{(0)}$ in (42) is all what we will need in obtaining the time-domain solution for an impedance-loaded transmission line with a voltage source.

To obtain the transient response of the total current in (41), we now apply the Fourier inverse transformation in (1.2). By deforming the contour of integration into the upper (lower) half of the ω-plane for $(t - t_o)$ smaller (larger) than (z-z'), we finally obtain the following SEM representation:

$$I_\ell(t,z,z') = \left(\frac{V_o}{R_o}\right)\left[Q_o + \sum_{s=-\infty}^{\infty} \frac{e^{-i\frac{\omega_s^\ell}{c}L}}{\omega_s^\ell F_s(d)D'(\omega_s^\ell)} F_s(z')F_s(z)e^{-i\omega_s^\ell(t-t_o)}\right]$$

$$H\left(t - t_o - \frac{z_> - z_<}{c}\right) \tag{45}$$

where the natural mode current $F_s(z)$ is given by (26). The constant Q_o in (45) is the residue at the pole, $\omega = 0$, of $\tilde{V}_g(\omega)$.

3.2.2 Numerical Results

In all of the following numerical examples, we assumed that the loaded transmission lines are terminated in open-circuit at both ends, i.e., $\Gamma_{t_1} = \Gamma_{t_2} = +1$, and we used up to the first fifty modes to compute the time response. The "early-time" response (i.e., before the first reflected wave from the end reaches the observation point) in each case was further compared with the first term in the "series method" solution (see Appendix B) to confirm its accuracy. In general, it was found that only first few modes are needed to achieve convergence and excellent accuracy for the "late-time" response. For the "early-time" response however, many terms in (45) are needed for an accurate result; nevertheless, we found a much faster convergence for the response of a $R_\ell - L_\ell$ loaded line than that of a $R_\ell - C_\ell$ loaded one. For the $R_\ell - L_\ell$ (center load) case, ten to fifteen (even) modes were generally found to be sufficient to yield accurate results for the "early-time" response.

Results for a center-loaded transmission line

a) $R_\ell - L_\ell$ loaded line:

Figures 17 - 21 show the driving-point current response of a series R_ℓ-L_ℓ center-loaded transmission line, center-driven by a voltage source, with a step-function time response. In Fig. 17, the responses of an inductive loaded line ($r = 0$), for two values of the inductive impedance x_L, are compared with that of the unloaded one. As we see, increasing the inductive impedance x_L, increases the time between two subsequent zero crossings of the current, indicating an effective lengthening of the line. One could expect this behavior from Fig. 5, because the natural frequencies for $x_L = 1$ (and $r = 0$) have smaller values than those of $x_L = 0.1$, causing the slower oscillation

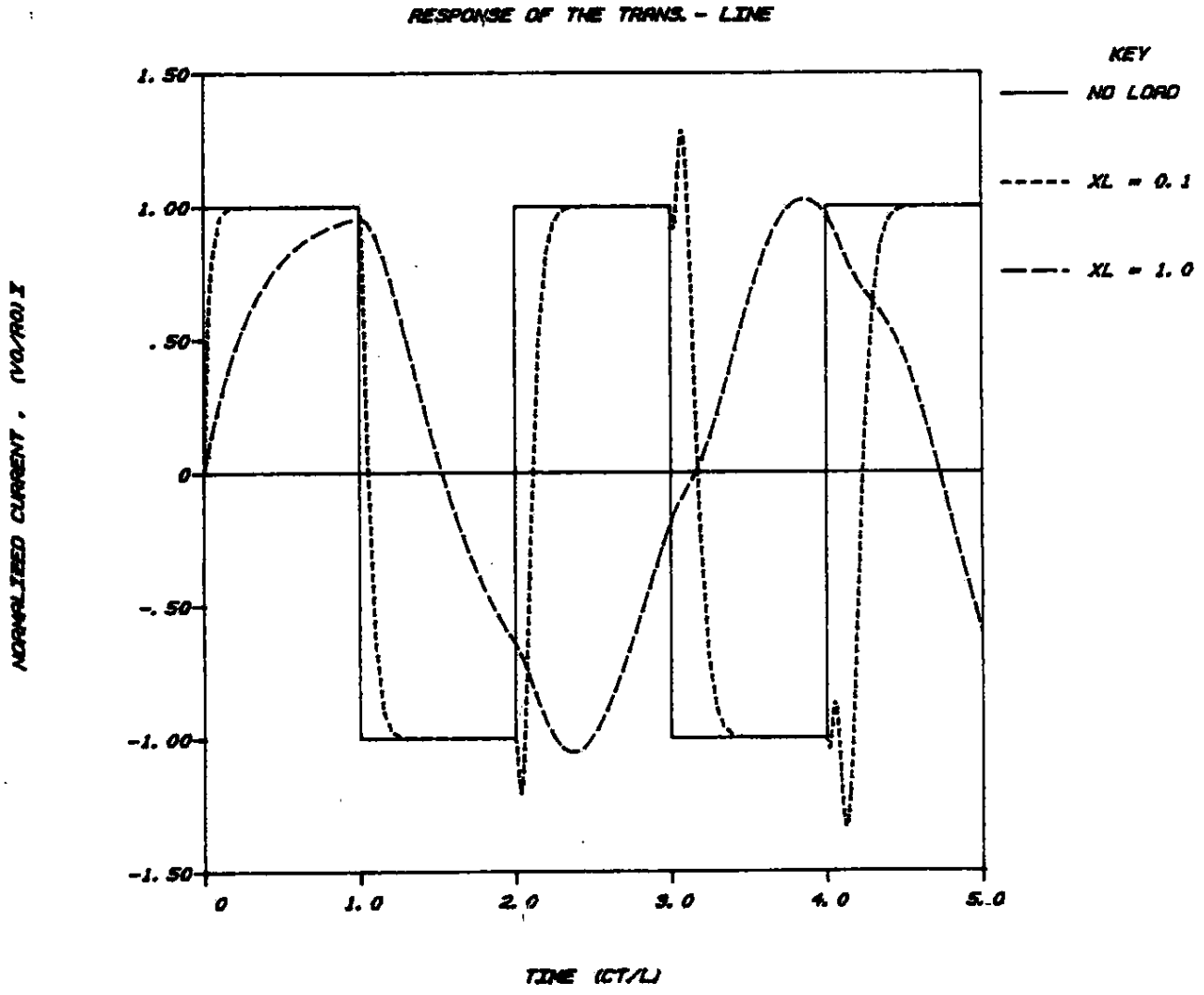

Fig. 17: Transient response of the driving-point current on an inductive center-loaded transmission line, center-driven by a voltage generator with output $V_0H(t)$.

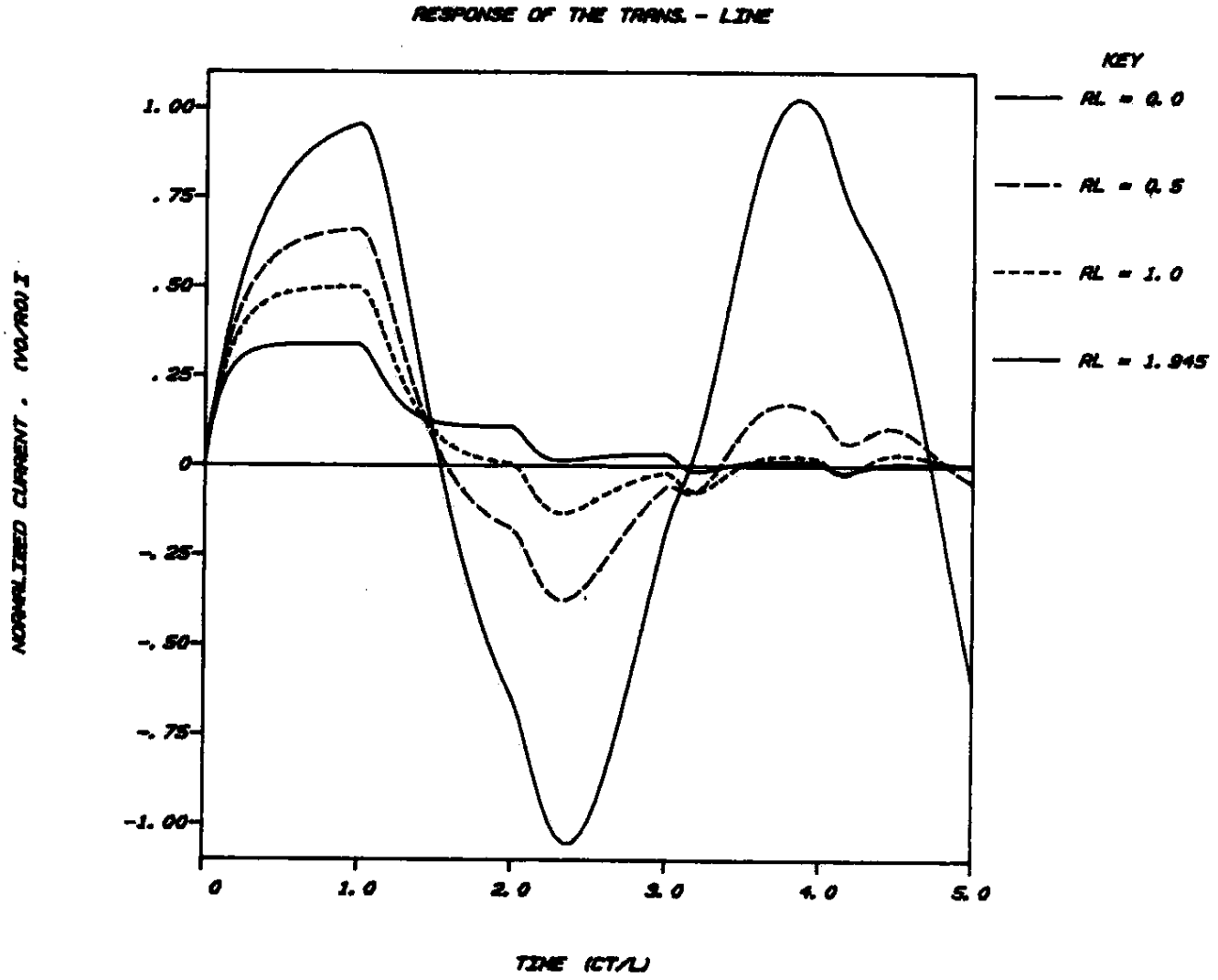

Fig. 18-a: Transient response of the driving-point current on a $R_\ell - L_\ell$ center-loaded transmission line, center-driven by a voltage generator with output $V_0 H(t)$; $x_L = 1$, $r < r_c \simeq 1.948$.

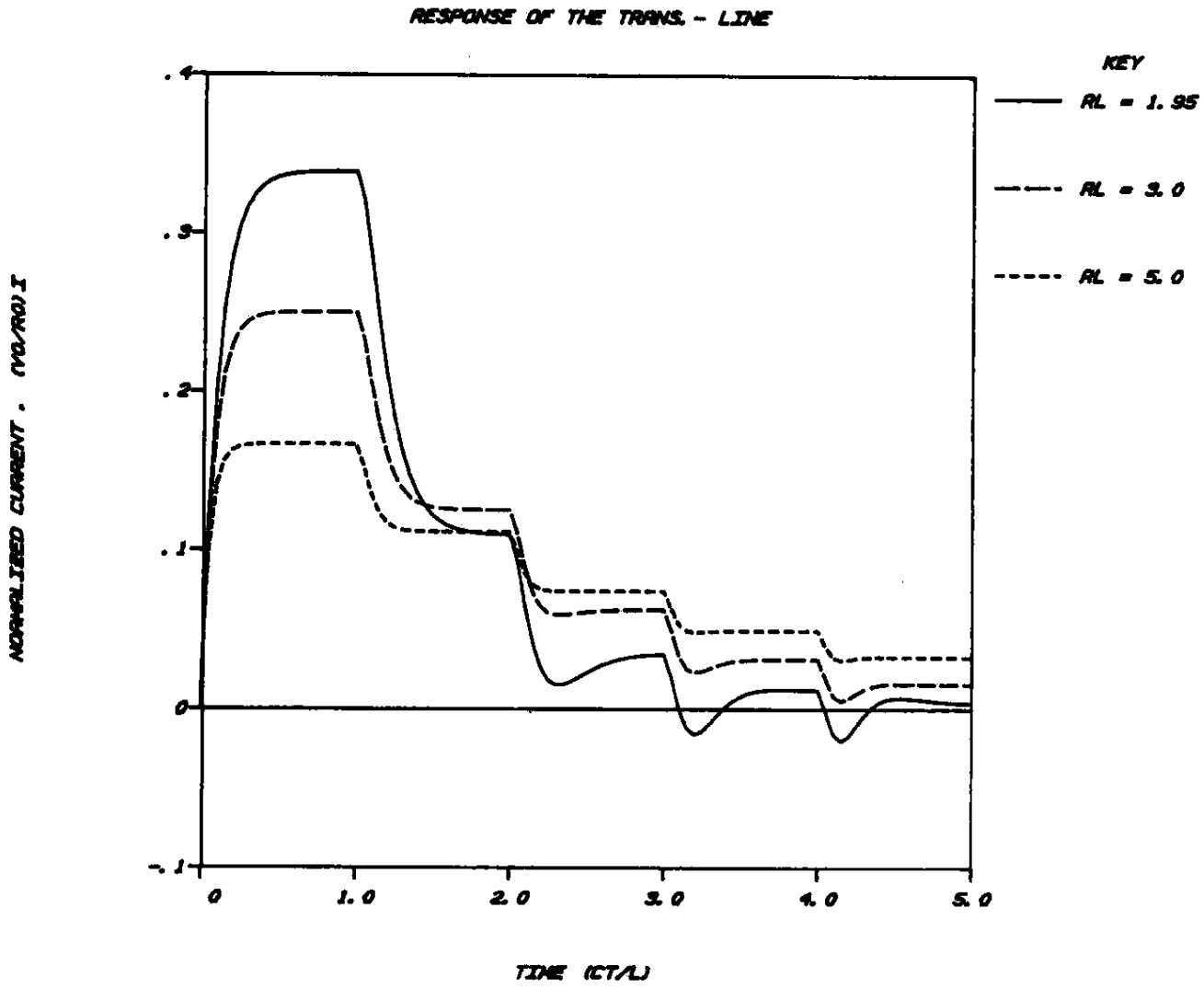

Fig. 18-b: Transient response of the driving-point current on a $R_\ell - L_\ell$ center-loaded transmission line, center-driven by a voltage generator with output $V_o H(t)$; $x_L = 1$, $r > r_c \simeq 1.948$.

in the time-domain. The rapid variations of the amplitude, for $x_L = 0.1$, in the vicinity of $\frac{ct}{L} \simeq 2,3,4,\ldots$, i.e., when the reflections from the ends reach the observation point, are also noticeable in Fig. 17. Figures 18-a and 18-b show the transient responses of a $R_\ell - L_\ell$ loaded line, for $x_L = 1$ and as the values of the normalized resistor r vary. We notice that initially, increasing r reduces the current amplitude and increases the "oscillation-period." For the values $r = 1.945$ and $r = 1.95$, which are extremely close to the "critical-load" r_c ($r_c \simeq 1.948$, see Fig. 5) of the lowest order mode, the response decays very fast in time and rapidly approaches zero for $\frac{ct}{L} \geq 2$ (i.e., after two reflections from the ends); this can be referred to as the "critically-damped" response, as was discussed earlier in section 3.1.2. For $r > r_c$ however, the current does not cross the time axis and decays very slowly in time as shown for $r = 3$ and 5 in Figure 18-b. By an analogy to the circuit theory [12], the transient response for $r > r_c$ ($r = 3$ and 5 in Figure 18-b) may be referred to as the "over-damped" response. Similarly, the transient current for $r < r_c$ ($r = 0$, 0.5, 1 in Fig. 18-a) may be called the oscillatory or the "underdamped" response.

In order to examine the contributions from the different SEM modes to the total response, we have included in Figures 19-21, the time-response of each mode. Unquestionably, the major contribution to the total current for $r \simeq 1.945$, i.e. near critical damping, comes from the first mode, which is much more efficiently excited than the higher order modes. It was found however, that for $r = 1.95$ (i.e., for r very close to, but larger than critical load, r_c), the two "evanescent' modes (corresponding to the two poles on the imaginary axis in Fig. 7) are the dominant components which have extremely large amplitudes, but substantially cancel each other to give the small total current shown in Fig. 18-b. As r increases however, the

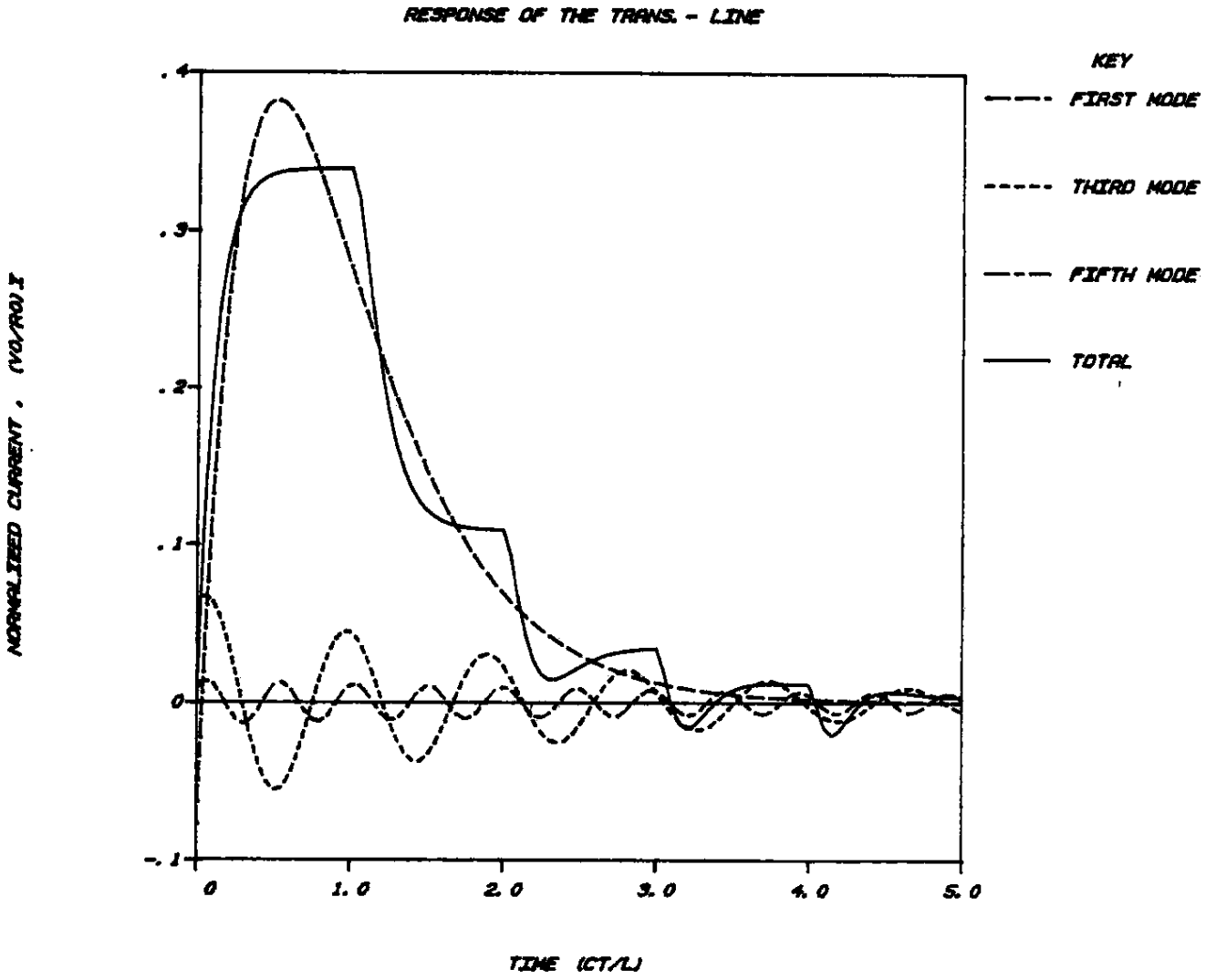

Fig. 19: Transient response of the driving-point current on a $R_\ell - L_\ell$ center-loaded transmission line, center-driven by a voltage generator with output $V_0 H(t)$; $x_L = 1$, $r = 1.945$.

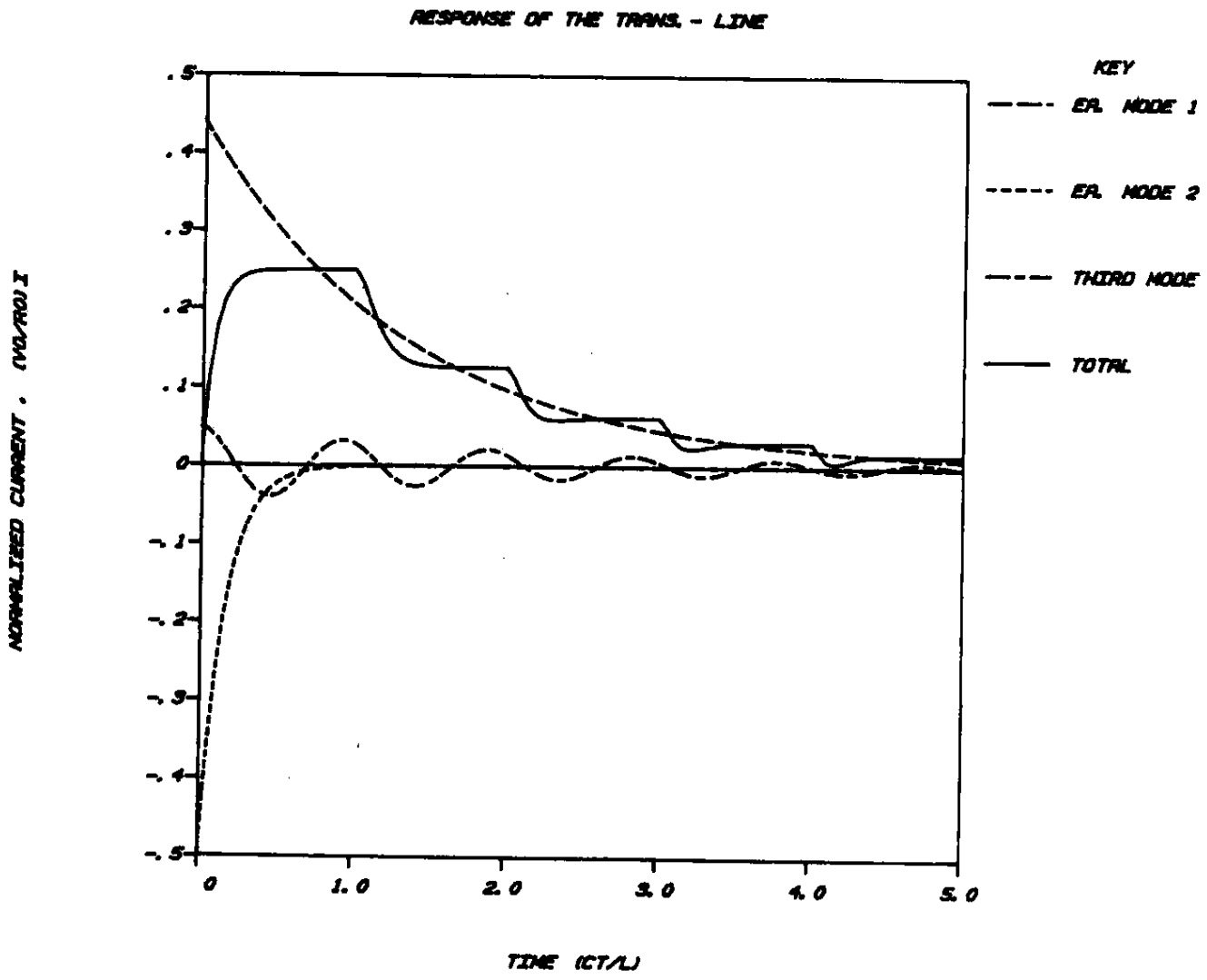

Fig. 20: Transient response of the driving-point current on a $R_\ell - L_\ell$ center-loaded transmission line, center-driven by a voltage generator with output $V_o H(t)$; $x_L = 1$, $r = 3$.

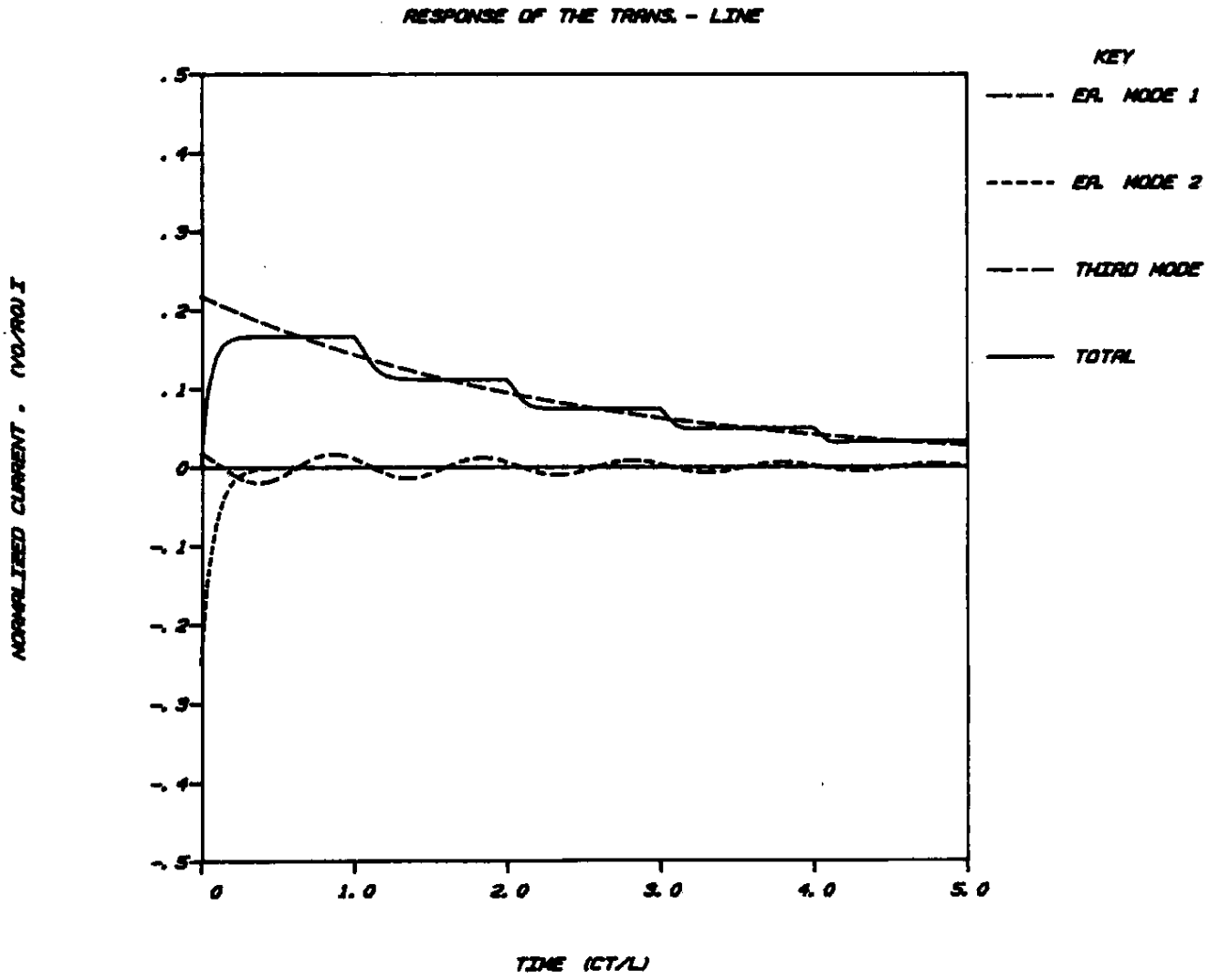

Fig. 21: Transient response of the driving-point current on a $R_\ell - L_\ell$ center-loaded transmission line, center-driven by a voltage generator with output $V_o H(t)$; $x_L = 1$, $r = 5$.

second "evanescent" mode which has a larger attenuation (see Figs. 5 and 13-b), contributes only in the very early times and decays very rapidly in time, as shown in Figs. 20 and 21 for r = 3 and 5, respectively. One can conclude from Figs. 19-21 that to calculate the total response for an R-L loaded line, with r close to the critical value of r_c as well as for $r > r_c$, only the first few natural modes are needed.

Transient responses of the current at $z = \frac{L}{2}$ and $z = \frac{3L}{4}$ for a $R_\ell - L_\ell$ center loaded line, driven by a voltage generator located at $z' = \frac{L}{4}$, are shown in Figs. 22 and 23. As can be seen in Fig. 22, there is no current at $z = \frac{L}{2}$ until $\frac{ct}{L} = 0.25$ at which time the incident current wave arrives, causing the response to rise up to a maximum. At $\frac{ct}{L} = 0.75$, the current wave reflected from the z = 0 end reaches the observation point at $z = \frac{L}{2}$ and causes the total current to drop. At $\frac{ct}{L} = 1.25$, the second set of the reflected waves arrive at the observation point. This set includes a "primary" wave reflected from the z = L end and a "secondary" current wave (i.e., an incident wave which is already reflected from the load at $d = \frac{L}{2}$) reflected at the z = 0 end. The repeat of the process at $\frac{ct}{L} = 1.75, 2, \ldots$ causes the damped oscillations in the total current. A similar discussion as above could be used to explain the transient behavior of the current at $z = \frac{3L}{4}$ in Fig. 23. However, contrary to the previous cases (i.e., Figs. 17-22), in computing the response in Fig. 23, the modes with odd distributions (i.e., $\frac{\omega_s L}{c\pi} = s$, s even), which do not "see" the center load, have also contributed to the total current at $z = \frac{3L}{4}$. Nevertheless, since the modes with the natural frequencies $\frac{\omega_s L}{c\pi} = s$, $s = 4, 8, 12, \ldots$, have zero amplitudes at $z = \frac{L}{4}$ and $\frac{3L}{4}$, they are not excited by the source at $z' = \frac{L}{4}$ and do not contribute to the total current at $z = \frac{3L}{4}$.

b) $R_\ell - C_\ell$ loaded line:

In Figures 24-28, the current response of a series R_ℓ-C_ℓ center-loaded

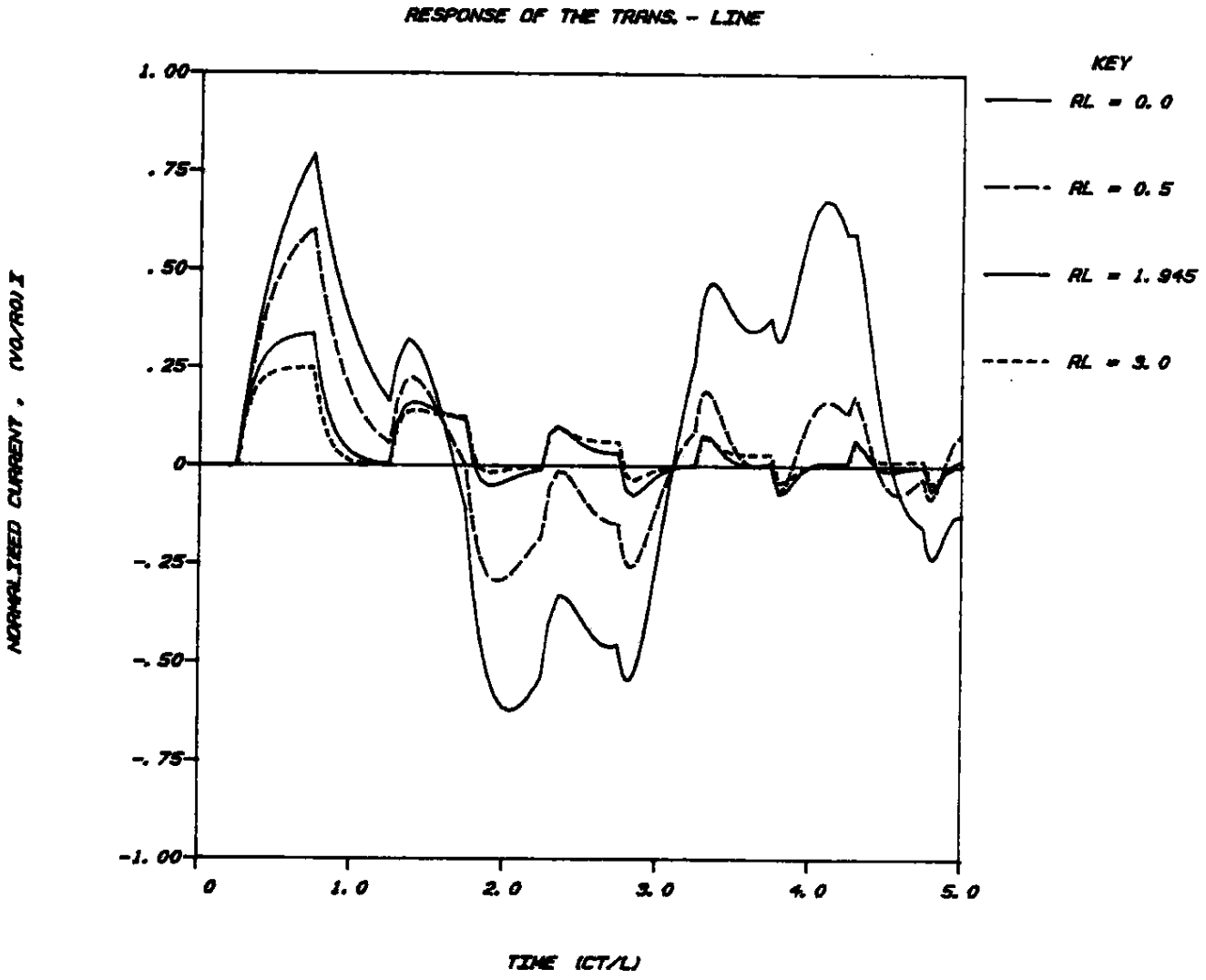

Fig. 22: Transient current response at $z = \frac{L}{2}$ on a $R_\ell - L_\ell$ center-loaded transmission line, driven at $z' = L/4$ by a voltage generator with output $V_0 H(t)$; $x_L = 1$, $r = 0, 0.5, 1.945, 3$.

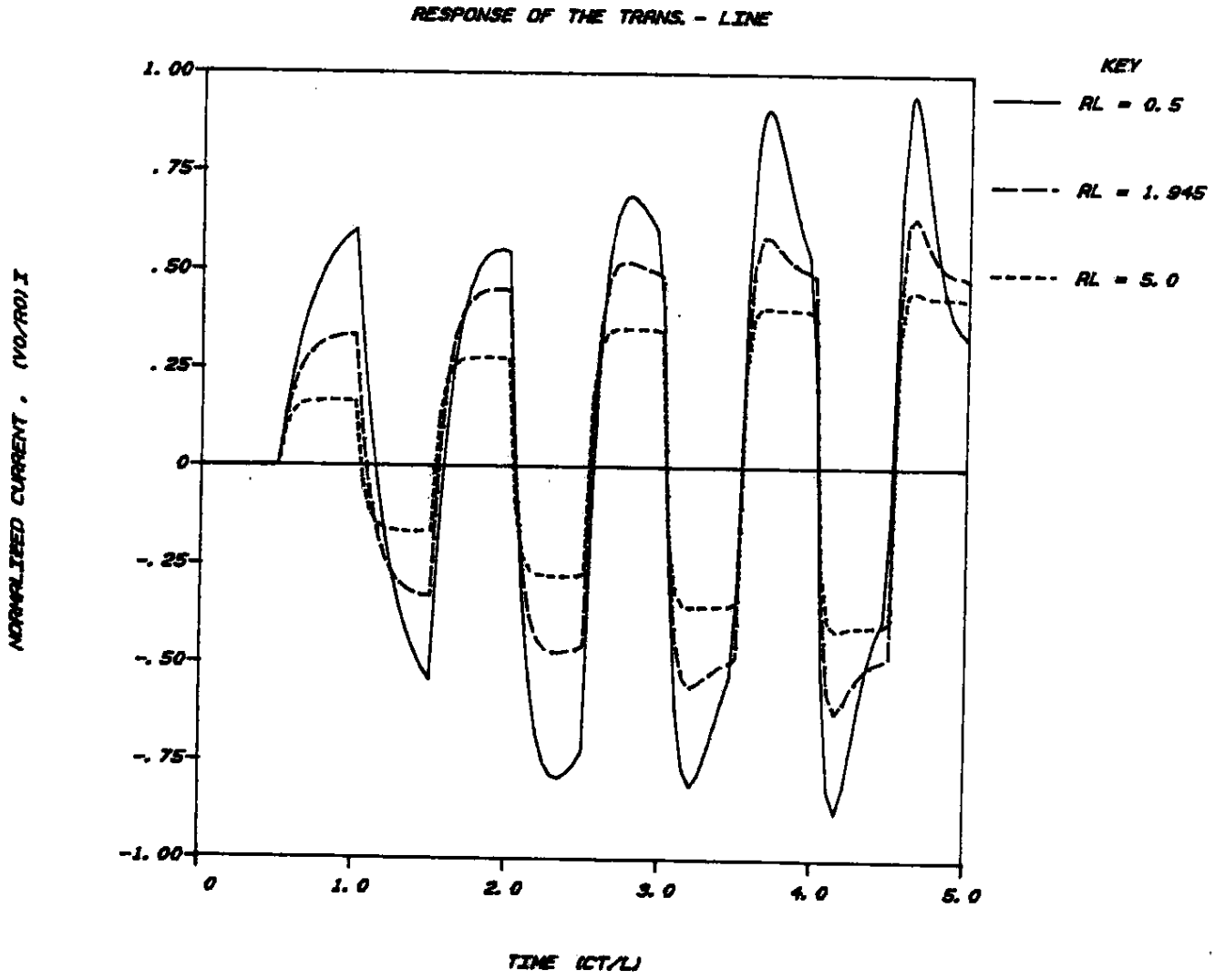

Fig. 23: Transient current response at $z = \frac{3L}{4}$ on a $R_\ell - L_\ell$ center-loaded transmission line, driven at $z' = L/4$ by a voltage generator with output $V_0 H(t)$; $x_L = 1$, $r = 0.5, 1.945, 5$.

line are plotted. The results are given for the normalized capacitive impedance, $x_c = 0.1$. Figure 24 shows the effect of the capacitive loading ($r = 0$) on the driving point current response of transmission line, center-driven by a voltage generator with a step-function time response, $V_g = V_o H(t)$. The capacitive load effectively shortens the line; this is the opposite effect of the inductive load in Fig. 17. Figure 25 shows the effects of adding a resistor in series to the capacitive load of Figure 24; as expected the resistive load reduces the current amplitude. In addition, at $r \simeq 1.05$ the current response rapidly approaches zero for $\frac{ct}{L} \geq 1$, where for $r = 2$ the response does not cross the time axis. To explain these latter behaviors, we have shown in Figure 26 and 27 the individual response of the first three modes. As shown for $r = 1.05$ in Fig. 26, the amplitudes of the evanescent and first modes are very large, but opposite in the sign for $\frac{ct}{L} \leq 0.25$. For $\frac{ct}{L} > 0.75$ however, the first mode is the dominant component and its large attenuation factor is responsible for the fast decay ("critical-damping") of the total current response for $\frac{ct}{L} > 1$. As r increases however, the first mode's excitation at $z = \frac{L}{2}$ becomes smaller and the evanescent mode now becomes the dominant component in the late time; and consequently, its sinh mode distribution causes the non-oscillatory (or "over-damped") behavior of the total current, as shown for $r = 2$ in Fig. 27.

Finally, the response of the $R_\ell - C_\ell$ center-loaded line, when the source and observation points are located at $z' = \frac{L}{4}$ and $z = \frac{L}{2}$, respectively, is shown in Figure 28. As expected, due to the time causality in summation in (45), the current is zero for $\frac{ct}{L} < 0.25$; also the effects of the reflections from the two ends of the line at $\frac{ct}{L} = 0.75, 1.25, \ldots$ can be clearly seen in this figure.

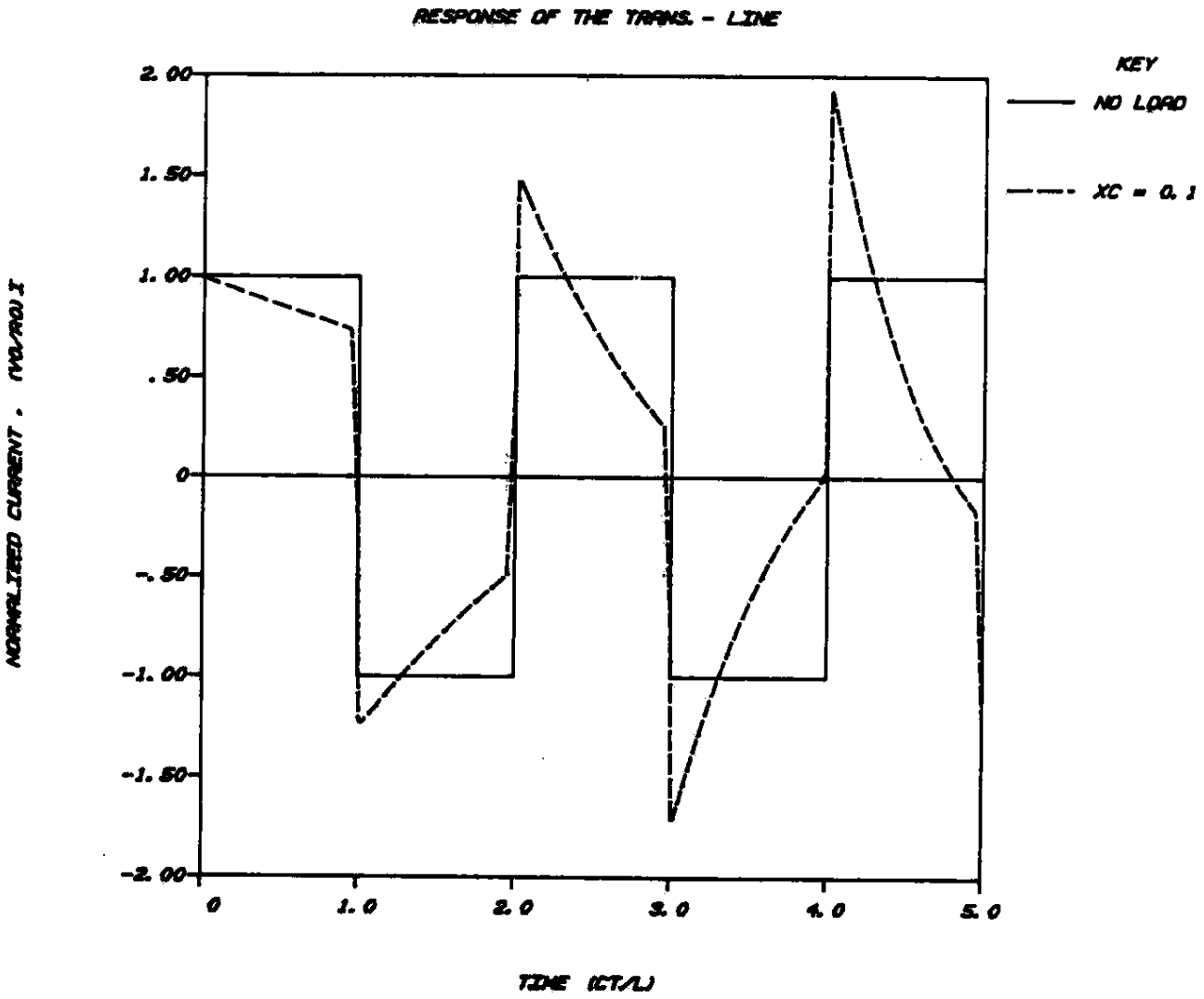

Fig. 24: Transient response of the driving-point current on a capacitive center-loaded transmission line, center-driven by a voltage generator with output $V_o H(t)$.

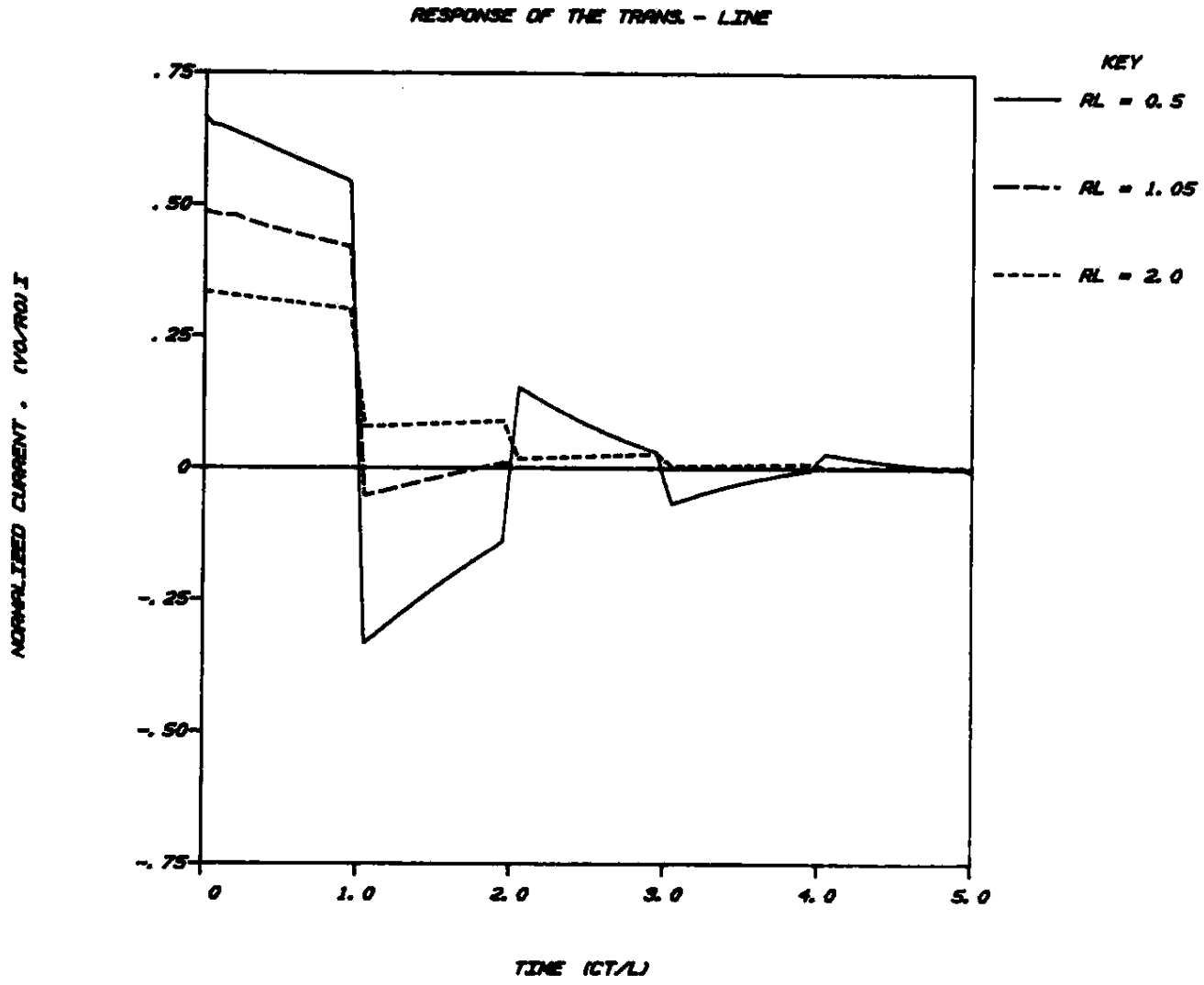

Fig. 25: Transient response of the driving-point current on a $R_\ell - C_\ell$ center-loaded transmission line, center-driven by a voltage generator with output $V_0 H(t)$; $x_c = 0.1$, $r = 0.5$, 1.05, 2.

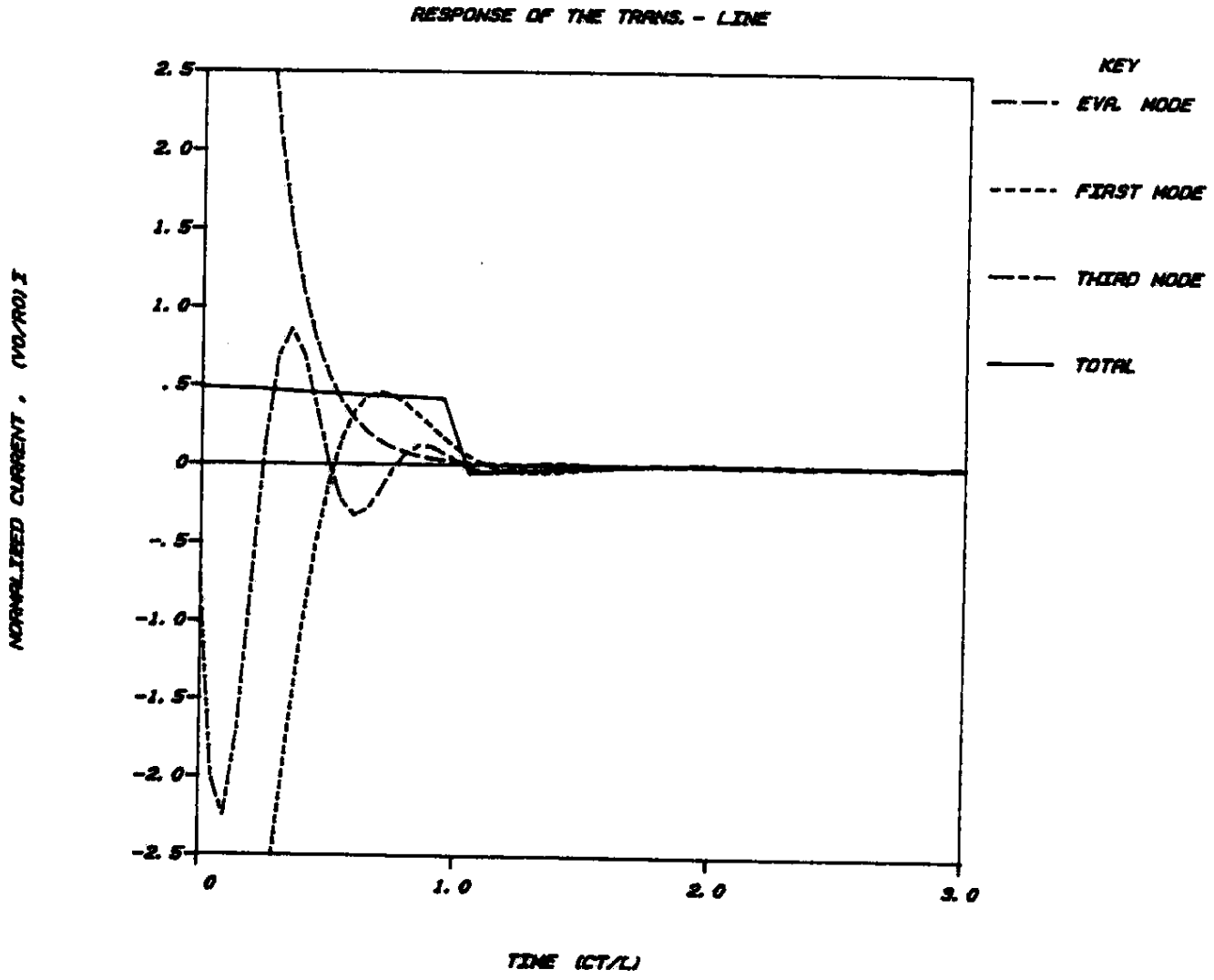

Fig. 26: Transient response of the driving-point current on a $R_\ell - C_\ell$ center-loaded transmission line, center-driven by a voltage generator with output $V_o H(t)$; $x_c = 0.1$, $r = 1.05$.

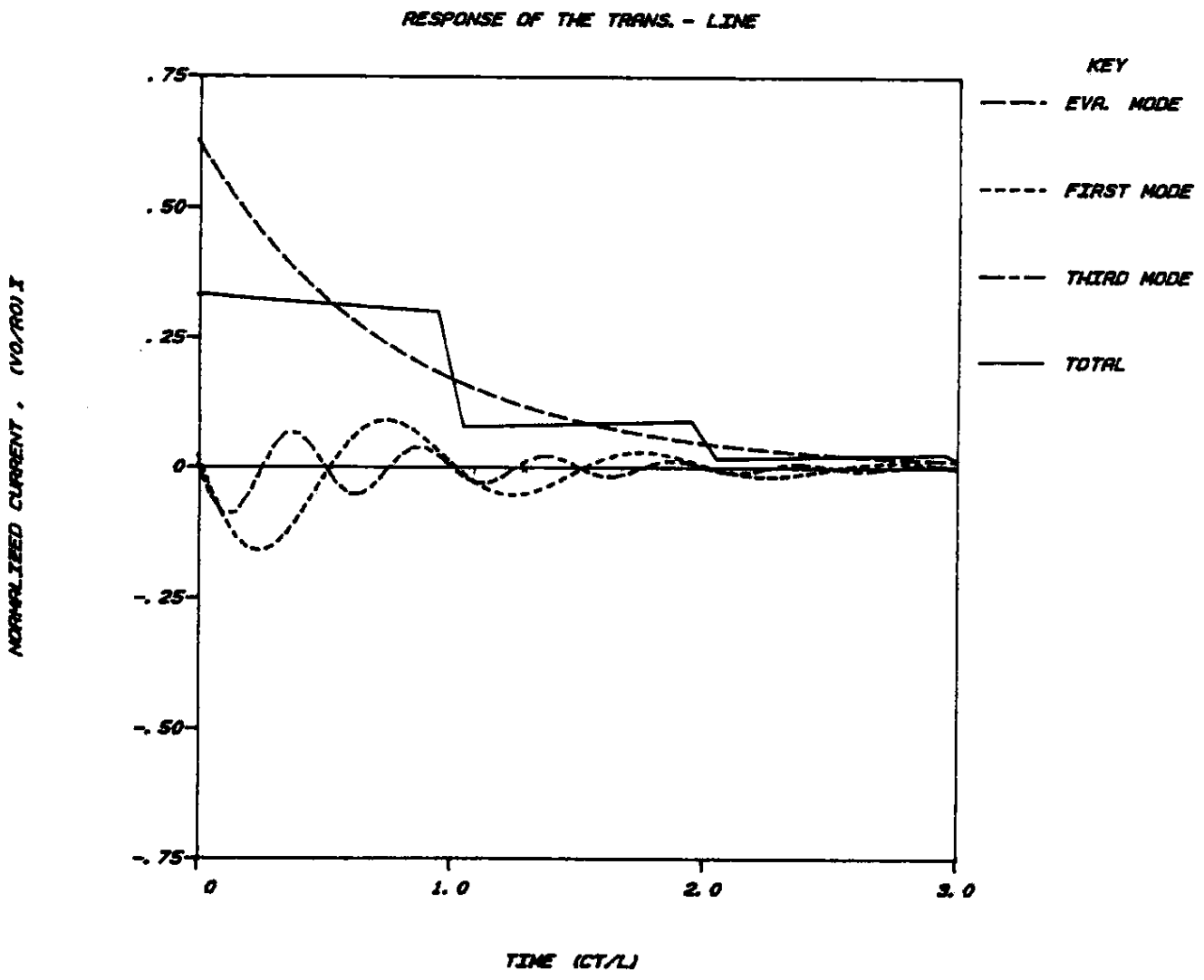

Fig. 27: Transient response of the driving-point current on a $R_\ell - C_\ell$ center-loaded transmission line, center-driven by a voltage generator with output $V_0 H(t)$; $x_c = 0.1$, $r = 2$.

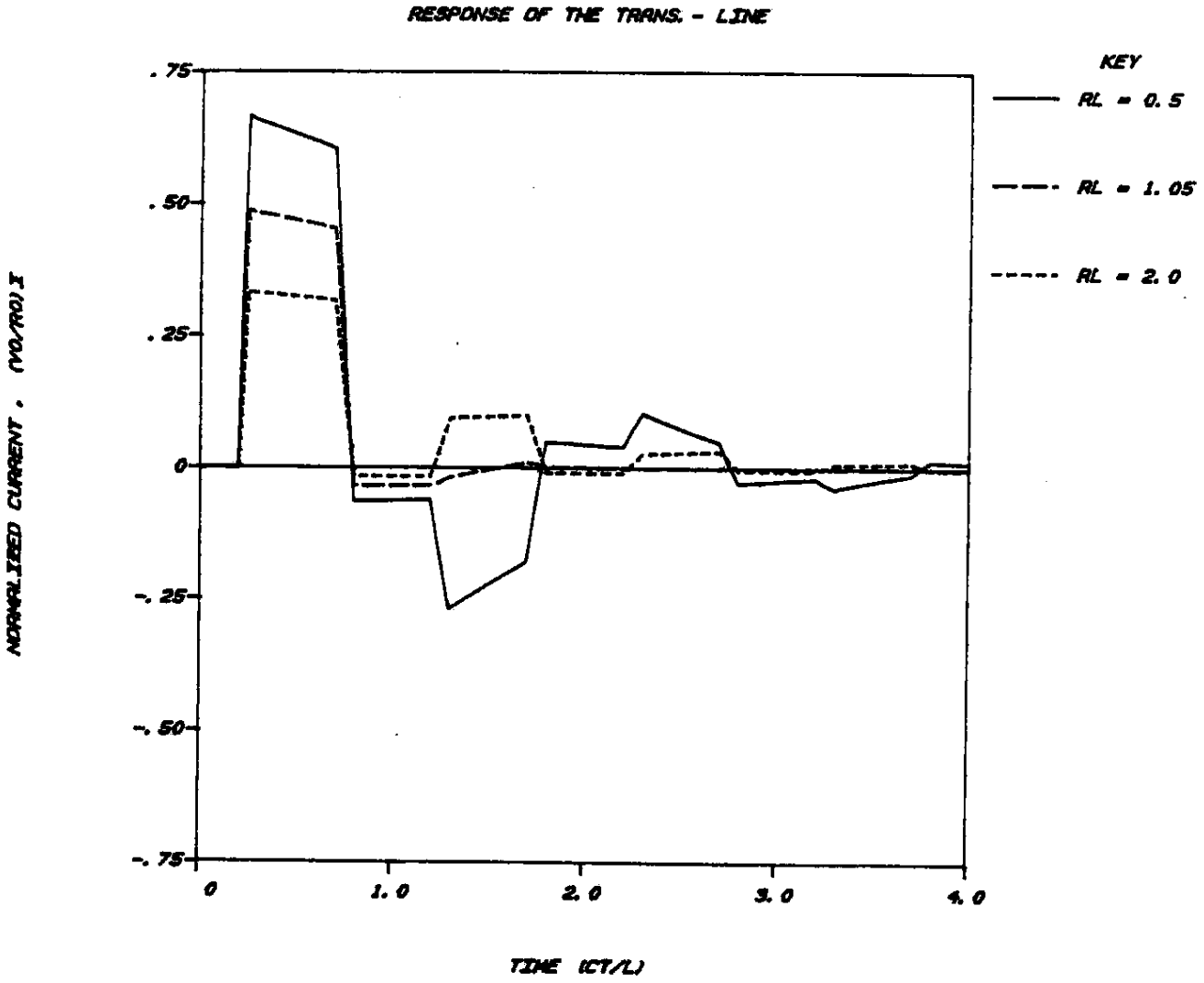

Fig. 28: Transient current response at $z = \frac{L}{2}$ on a $R_\ell - C_\ell$ center-loaded transmission line, driven at $z' = L/4$ by a voltage generator with output $V_0 H(t)$; $x_c = 0.1$, $r = 0.5, 1.05, 2.$

Results for an off-center loaded transmission line

To show the transients on an off-center loaded transmission line, the representation in (45) was used to calculate the current response of a $R_\ell - C_\ell$ loaded line with $x_c = 0.1$, $d = 0.35L$ and $z' = 0.65L$. The results are shown in Figs. 29-31 for the observation points, $z = 0.35L$ and $z = 0.65L$, respectively. For the response at $\frac{z}{L} = 0.35$ in Fig. 29, increasing r reduces the current's amplitude; nevertheless the response at $r = 1$ decays more rapidly for $\frac{ct}{L} > 2$, than that at $r = 2$, as one might expect from its sinh distribution in Fig. 15-b. For the response at $\frac{z}{L} = 0.65$ in Fig. 30, the normalized current, for all values of r, is one until $\frac{ct}{L} = 0.6$ at when the reflected current wave from the load at $\frac{d}{L} = 0.35$ reaches the observation point. For $\frac{ct}{L} > 0.6$ however, increasing the values of r increases the amplitude; this is because as r becomes larger, the "load reflection coefficient," Γ_ℓ, gets closer to one, and consequently a substantial part of the incident wave reflects back toward the observation point. In fact, as r approaches infinity, $\Gamma_\ell \to 1$ and the observation point "sees" the point $\frac{d}{L} = 0.35$, as the end of a shorter line having the length 0.65L. It is obvious that for $r = \infty$, the response will be identical (but with the oscillation period $\frac{ct}{L} = 1.3$ instead of 2) to that shown in Figure 24, for no load case. Finally in Fig. 31, the individual time responses of the first three modes for the $r = 2$ load of Fig. 30 are shown. It can be seen that the first mode is the dominant component of the total current, while the "evanescent mode" contributes only in the early times. The second mode is very weakly excited, as one might have expected from the behavior of its natural mode distribution in Fig. 15-b. Although not shown in Fig. 31, but we found the third and fifth modes to be more strongly excited than the second and fourth ones. In general,

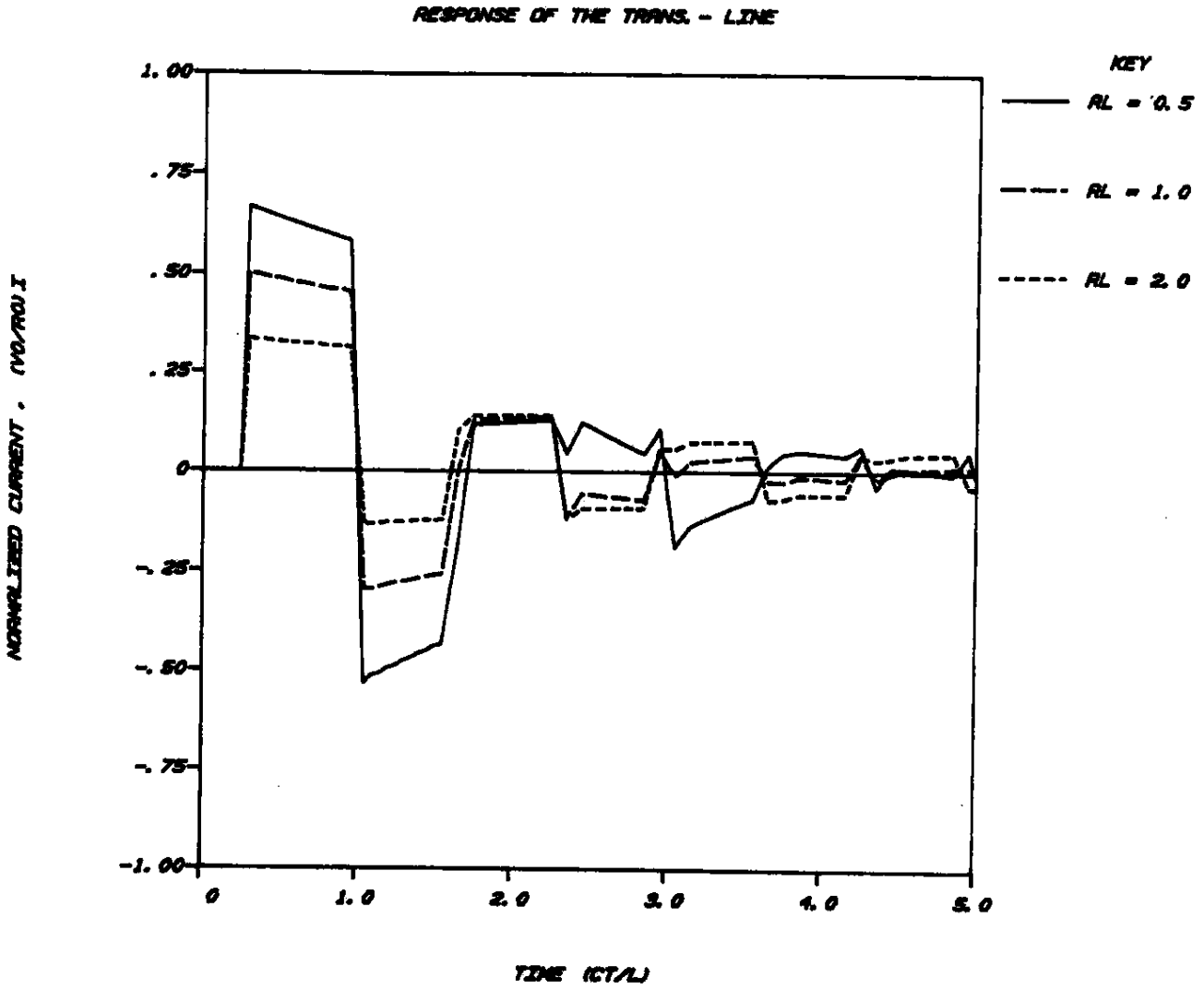

Fig. 29: Transient current response at $z = 0.35L$ on a transmission line, loaded at $d = 0.35L$ with a $R_\ell - C_\ell$ impedance and driven at $z' = 0.65L$ by a voltage generator with output $V_o H(t)$; $x_c = 0.1$, $r = 0.5, 1, 2$.

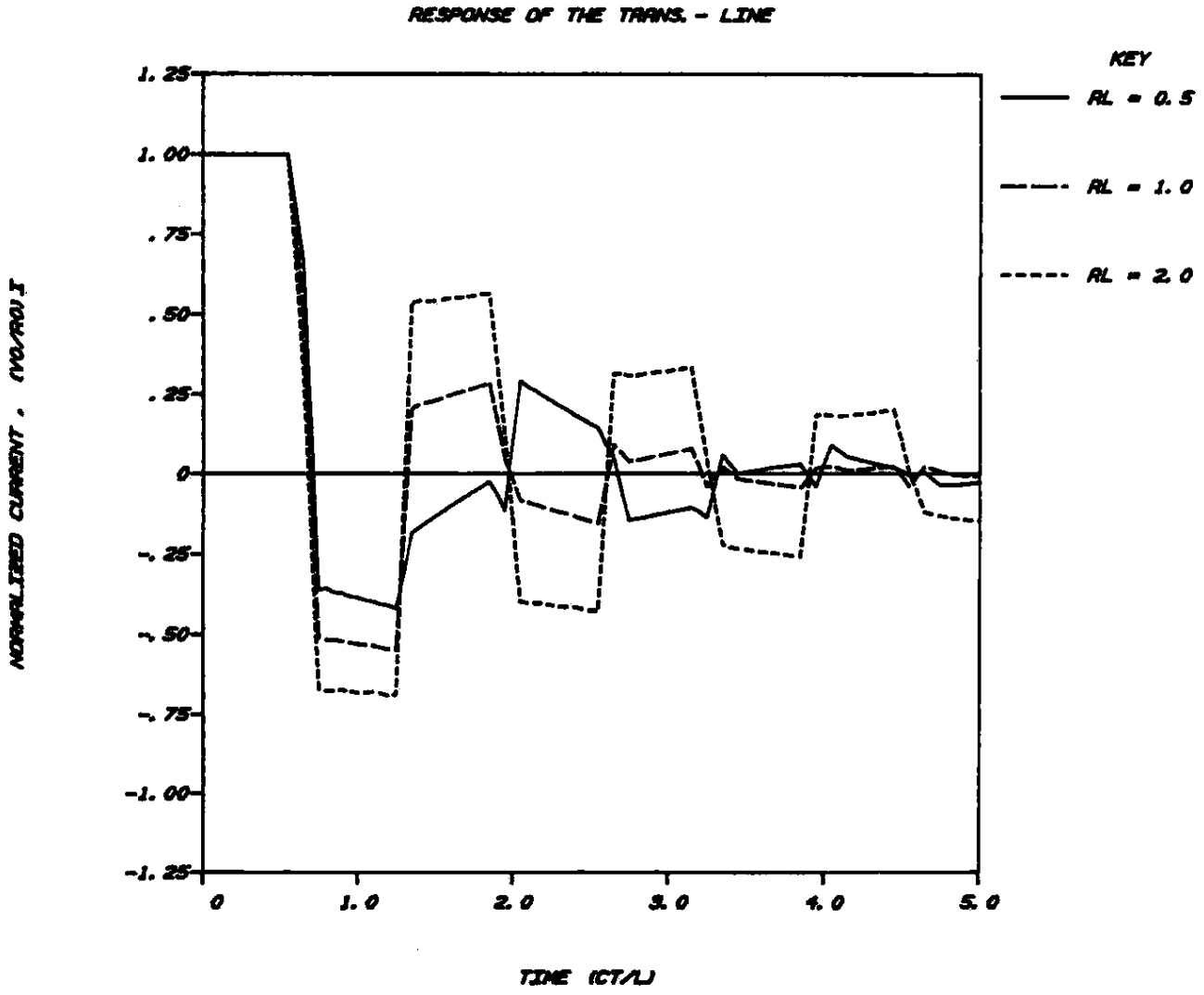

Fig. 30: Transient response of the driving-point current on a transmission line, loaded at d = 0.35 L with a $R_\ell - C_\ell$ impedance and driven at z' = 0.65L by a voltage generator with outout $V_o H(t)$; x_c = 0.1, r = 0.5, 1, 2.

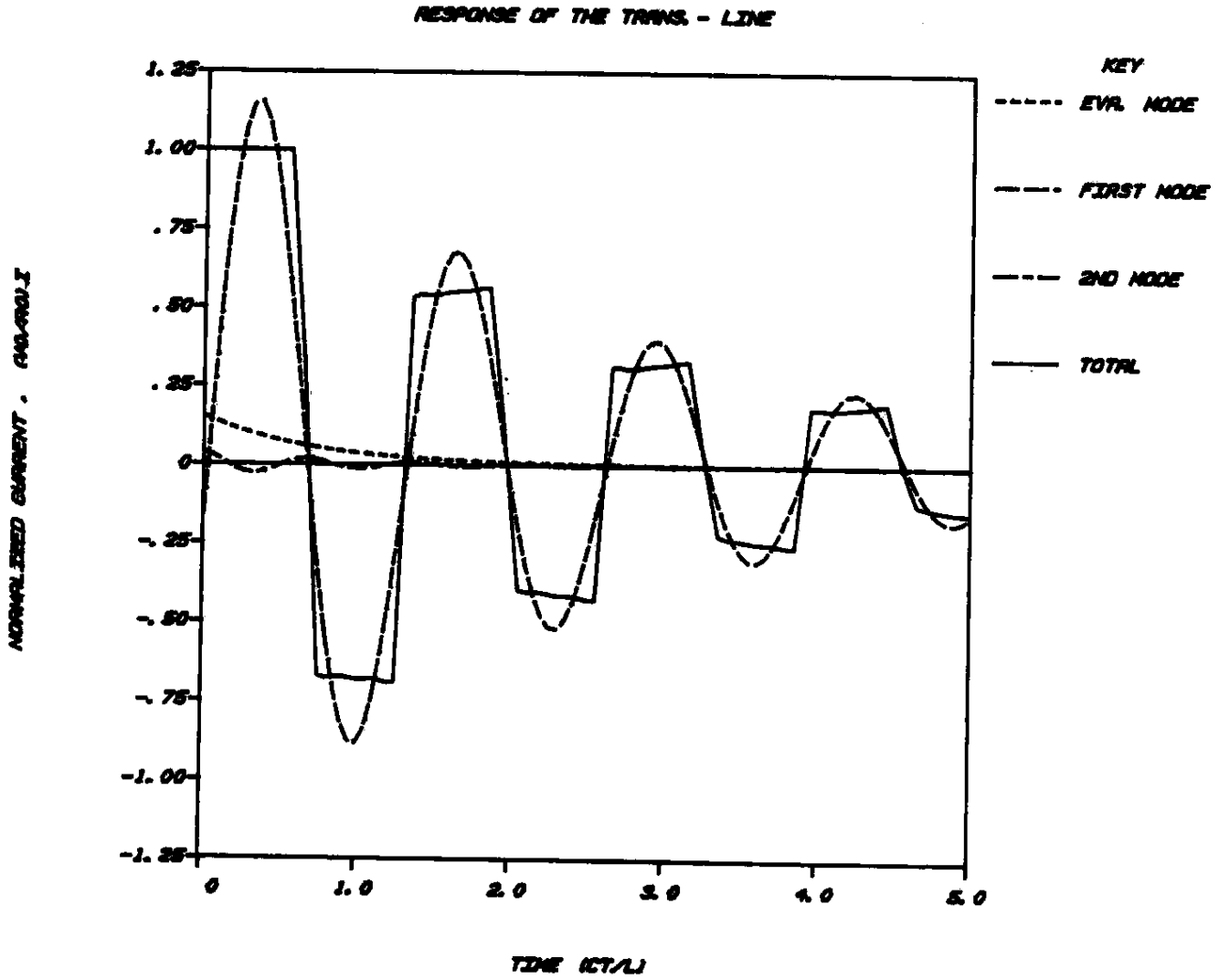

Fig. 31: Transient response of the driving-point current on a transmission line, loaded at d = 0.35L with a $R_\ell - C_\ell$ impedance and driven at z' = 0.65L by a voltage generator with output $V_0 H(t)$; $x_c = 0.1$, $r = 2$.

since the source and observation points are both located at $\frac{z}{L} = 0.65$, only the "first set" of natural modes, s = 1,3,5,... effectively contribute to the total response, as was discussed in section 3.1.2.

Before concluding this section, it is worthy to mention that the SEM solution in (45) was found to be more appealing than the "conventional" series method for calculating the "late-time" response. Because the only time-dependent term in the summation in (45) is that of $e^{-i\omega_s t}$, therefore once the first several natural frequencies and modes distributions are evaluated, they can easily be used to compute the current responses at any value of t. As was discussed earlier, the convergence of the summation in (45) for "early-time" is generally slow; however, the response of a finite transmission line for the "early-times" (i.e., before the first reflected wave from the ends reaches the observation point) is identical to that of an infinite line. Subsequently, the simple expressions which can be easily obtained for a loaded infinite line may be used to calculate the "early-time" responses of the corresponding loaded finite transmission lines. Those expressions for various impedance loads are given by (B.6) - (B.9) in Appendix B.

4. CONCLUSION

The SEM modes behaviors and the transient responses of various impedance loaded transmission lines were studied in this report.

In general, it was shown in section 3.1 that the corresponding natural frequencies of the R_ℓ - C_ℓ and R_ℓ - L_ℓ loaded lines move transversely in the opposite directions in the complex ω-plane as the values of $r = \frac{R_\ell}{R_o}$ vary from 0 to ∞. In addition, the nature of the "evanescent mode" for R_ℓ - C_ℓ and $R_\ell \| C_\ell$ loaded lines, and the occurrence of a "double pole" on the imaginary axis for R_ℓ - L_ℓ as well as modal degeneracies for (R_ℓ, L_ℓ, C_ℓ) loaded-lines, were discussed. It was also shown that for an off-center loaded line, there are two different sets of natural modes which resonate predominantly in the two segments of the line, separated by the load.

In section 3.2, the corresponding SEM representation for the transient current response of the loaded transmission line of section 3.1 was derived. It was shown that only a part of the frequency-domain response ($\tilde{I}_\ell^{(0)}$ in (42)) of a transmission line with an arbitrarily-located load, contributes to the final SEM representation for the time-domain response. The numerical results for the transient current response, for various load parameters and locations as well as various source and observation points, were presented. The "critically-damped" as well as the so-called "under-damped" and "over-damped" transmission lines were also defined in this section, and their transient responses were interpreted and explained through the behaviors of the corresponding natural frequencies, in the complex ω-plane, and modes distributions along the line. In particular, it was shown that for a R_ℓ - L_ℓ center-loaded line with open-circuit terminations, the (load) current response will be "critically-damped" if $r \simeq r_c$ where r_c is the critical resistor, corresponding to the critical natural frequency (i.e., the "double pole") which satisfies the equation (35).

The "under-damped", or oscillatory, and the "over-damped", or non-oscillatory responses occur for $r < r_c$ and $r > r_c$, respectively.

The numerical results and discussions in section 3.2.2 demonstrated that how the behaviors of the natural frequencies and modes in section 3.1 could be used to predict the corresponding behavior of the transient response of the transmission line. This provides an effective tool in the design and synthesis of the loaded transmission lines.

The time-domain SEM representations (12) and (45) were obtained for an excitation wave form of a time unit step-functions only. When the excitation voltage $\tilde{V}_g(\omega)$ has pole singularities besides the one at $\omega = 0$, the corresponding transient response can be determined by simply adding the residues' contributions at these poles to those at the SEM poles. In that case the corresponding P_o and Q_o functions in (12) and (45) will be exponentially time-dependent. It should also be mentioned that all of the numerical results in section 3.1.2 and 3.2.2 were presented only for the open-circuit terminated lines because of our desire to interpret the SEM properties of a loaded thin-wire antenna. It can easily be explained from the modeal equation (27.2) that for a <u>short-circuit</u> termination, the natural frequencies for a $R_\ell - L_\ell$ center-loaded line, behave like those in Fig. 4, while for a $R_\ell - C_\ell$ center-load, the behavior is similar to those in Fig. 5. These behaviors are the opposite of those corresponding to an open-circuit termination, as one might expect.

Finally, by studying the present problem, a number of similarities between the SEM modal behavior of a loaded transmission line and that of a loaded thin-wire antenna was uncovered. For example, it was found that the natural frequencies of a resistively loaded thin-wire cylindrical antenna, in the

complex ω-plane, behave like those of a $R_\ell \| C_\ell$ loaded line. By an analogy, one may expect that the natural frequencies of a resistively loaded thin-wire circular loop behaves like those of a (R_ℓ , L_ℓ) loaded line. Furthermore, any modal degeneracies, critical-damping, etc., which was discussed for various loaded transmission lines in section 3, can also be expected for properly loaded thin-wire antennas. Therefore the results presented in this work not only explain physically some of the SEM modal behaviors of the loaded antennas, but also will establish foundations which will give clues to what changes one may expect (in the complex ω-plane, mode distributions, etc.) if the load combination, parameters or location is varied. Then, after the changes, according to the rough "transmission-line model" are desirable, one may proceed with the more involved and time consuming computations for the corresponding antenna problem.

As a concluding remark, it should be mentioned that the SEM analysis presented in this work can be easily extended to formulate the transient SEM representation of a lossy transmission line. A brief formulation of this latter problem is given in [6, Appendix D]. A more detailed analysis together with the corresponding numerical results will be presented in a future report.

References

[1] Levinson, N., "The Fourier transform solution of ordinary and partial differential equations," J. Math. Phys., vol. 14, pp. 195-227, 1935.

[2] Bewley, L.V., Traveling Waves on Transmission Systems, 2nd Ed. John Wiley and Sons, New York, 1951.

[3] Weber, E., Linear Transient Analysis, Volume II, John Wiley and Sons, New York, 1956, Chapters 6, 7 and 8.

[4] Kuznetsov, P.I. and R.L. Stratonovich, The Propagation of Electromagnetic Waves in Multiconductor Transmission Lines, MacMillan, New York, 1964.

[5] Tai, C.T., "Transients on lossless terminated transmission lines," IEEE Trans. Ant. Prop., Vol. 26, No. 4, pp. 556-561, July 1978.

[6] Hoorfar, A. and D.C. Chang, "Analytic determination of the transient response of a thin-wire antenna based upon a SEM representation, Part I: Unloaded Antenna," Sci. Rept. No. 55, Electromagnetics Lab., Dept. of Elec. Engineering, Univ. of Colorado, Boulder, CO, July 1981.

[7] Hoorfar, A. and D.C. Chang, "Analytic determination of the transient response of a thin-wire antenna based upon a SEM representation, Part II: Loaded Antenna," Sci. Rept. No. 56 (To be published).

[8] Tai, T.T., "Complex singularities of the impedance functions of antennas," Electromagnetics, Vol. 1, No. 4, pp. 443-453, Oct.-Dec. 1981.

[9] Ramo, S., J.R. Whinnery and T.V. Duzer, Fields and Waves in Communication Electronics, John Wiley and Sons, 1965, pp. 44-48.

[10] Whittaker, E.T. and G.N. Watson, A Course of Modern Analysis, 4th Ed. Cambridge University Press, London, 1973, pp. 134-136.

[11] Schelkunoff, S.A., "Theory of antennas of arbitrary size and shape," Proc. IRE, Vol. 29, pp. 493-521, Sept. 1941.

[12] Pearson, S.I., and G.I. Maler, Introductory Circuit Analysis, John Wiley and Sons, New York, 1965, pp. 92-97.

APPENDIX A

In this Appendix, the expansion of the frequency-domain current response of a transmission line in terms of its natural frequencies by means of Mittag-Leffler theorem is presented; and an inherent difficulty in the final time-domain response arising from the use of this theorem is discussed.

According to Mittag-Leffler theorem [10], if a function $f(x)$ is bounded at infinity and analytic at the origin, it can be expanded into a residue series in terms of its poles,

$$f(x) = f(0) + \sum_{n=1}^{\infty} r_n \left(\frac{1}{x - x_n} + \frac{1}{x_n} \right) \tag{A.1}$$

where x_n is a simple pole of $F(x)$ and r_n is the corresponding residue at this pole, i.e., $r_n = \lim_{x \to x_n} [(x - x_n) f(x)]$.

Let us now consider the current distribution given in (5), which can also be written as

$$\tilde{I}(\omega;z,z') = \tilde{V}_0(\omega)\, Y(\omega;z,z') \tag{A.2}$$

where

$$Y(\omega;z,z') = \frac{1}{R_0} \cdot \frac{e^{-j\frac{\omega}{c}L}}{\Delta(\omega)}\, g_1(\omega;L - z_<) g_2(\omega;z_>) \tag{A.3}$$

We now apply the Mittag-Leffler theorem to the "admittance" function $Y(\omega;z,z')$ and expand (A.3) in terms of the natural frequencies ω_s, $s = 0, \pm 1, \pm 2, \ldots$ which are the zeros of $\Delta(\omega)$ in (9). Then, according to (A.1) and after some simplification, finally we have

$$Y(\omega;z,z') = Y(0;z,z') + \frac{1}{R} \sum_{s=-\infty}^{\infty} \left(\frac{1}{\omega - \omega_s} + \frac{1}{\omega_s} \right) \frac{\Gamma_{t_1}(\omega_s)}{\Delta'(\omega_s)}\, G_s(z) G_s(z') \tag{A.4}$$

provided that $Y(\omega;z,z')$ does not possess any pole at $\omega = 0$. In (A.4), $G_s(z)$ is the natural mode current given by (15). If Y is not analytic at the origin, i.e., has pole at $\omega = 0$, one may subtract out this pole singularity from (A.3) and apply the theorem in (A.1) to the remaining analytic part.

The SEM representation for the frequency-domain current is now given by (A.2) with $Y(\omega;z,z')$ expressed in (A.4). For a step-function excitation $\tilde{V}_0(\omega) = \frac{iV_0}{\omega}$, and the representation is given by

$$\tilde{I}(\omega;z,z') = \frac{iV_0}{\omega} Y(0;z,z') + \frac{iV_0}{R_0} \sum_{s=-\infty}^{\infty} \left(\frac{1}{\omega-\omega_s}\right) \frac{\Gamma_{t_1}(\omega_s)}{\omega_s \Delta'(\omega_s)} G_s(z)G_s(z') \tag{A.5}$$

By performing the Fourier inverse transformation given in (1.2), we finally get the following time-domain SEM representation

$$I(t,t_0;z,z') = \frac{V_0}{R_0}\left[P_0 + \sum_{s=-\infty}^{\infty} \frac{\Gamma_{t_1}(\omega_s)}{\omega_s \Delta'(\omega_s)} G_s(z)G_s(z')e^{-i\omega_s(t-t_0)}\right]H(t-t_0) \tag{A.6}$$

where

$$P_0 = \frac{[1-\Gamma_{t_1}(0)][1-\Gamma_{t_2}(0)]}{1-\Gamma_{t_1}(0)\Gamma_{t_2}(0)} \quad . \tag{A.7}$$

The expression in (A.6) is identical to the representation in (12) except for the argument of the unit-step function, H. The step-function in (12) explicitly demonstrates the time causality, which requires the total current response to be zero for $t - t_0 < \frac{z_> - z_<}{c}$. In (A.6) however, an extremely large number of terms are needed for convergence of the current response, to zero for $t - t_0 < \frac{z_> - z_<}{c}$.

APPENDIX B

In this Appendix, we present the so-called "series-method" formulation for the transient response of the impedance terminated transmission line of Figure 1-a.

From (5), the current in the real frequency domain is given by

$$\tilde{I}(\omega;z,z') = \left(\frac{iV_o}{\omega R_o}\right)\frac{e^{-i\frac{\omega}{c}L}}{\Delta(\omega)}\, g_1(\omega;L-z_<)\; g_2(\omega;z_>) \qquad (B.1)$$

where $g_{1,2}$ and $\Delta(\omega)$ are given by (6) and (9) respectively. But Taylor series expansion of the denominator in (B.1) yields

$$\frac{1}{\Delta(\omega)} = \left(1 - \Gamma_{t_1}\Gamma_{t_2}e^{i\frac{2\omega}{c}L}\right)^{-1}$$

$$= 1 + \Gamma_{t_1}\Gamma_{t_2}\, e^{i\frac{2\omega}{c}L} + (\Gamma_{t_1}\Gamma_{t_2})^2 e^{i\frac{4\omega}{c}L} + \ldots \qquad (B.2)$$

where the reflection coefficients Γ_{t_1} and Γ_{t_2} are given by (7). By applying the Fourier inverse transformation given in (1.2), we then have

$$I(t;z,z') = \left(\frac{iV_o}{2\pi R_o}\right)\int_{-\infty}^{\infty} \frac{1}{\omega}\left[e^{i\frac{\omega}{c}L_o} - \Gamma_{t_1}e^{i\frac{\omega}{c}L_1} - \Gamma_{t_2}e^{i\frac{\omega}{c}L_2} + \Gamma_{t_1}\Gamma_{t_2}\, e^{i\frac{\omega}{c}L_3}\right]\left[1 + \Gamma_{t_1}\Gamma_{t_2}e^{i\frac{2\omega}{c}L} + (\Gamma_{t_1}\Gamma_{t_2})^2 e^{i\frac{4\omega}{c}L} + \ldots\right] e^{-i\omega(t-t_o)}\, d\omega \qquad (B.3)$$

where

$L_o = z_> - z_<$, $L_1 = z_> + z_<$, $L_2 = (L - z_<) + (L - z_>)$ and

$L_3 = (L - z_>) + (L + z_<)$.

It is evident that the integrand in (B.3) contains an incident current wave eminating from the voltage source at $z = z'$ and an infinite number of reflected currents eminating from each end of the transmission line. By integrating each term of the integrand separately, one obtains the following "series-method" representation

$$I(t;z,z') = \frac{iV_o}{2R_o} \sum_{m=0}^{\infty} \Big[U_{m,m}(t;L_o + 2mL) - U_{m',m}(t;L_1+2mL) - U_{m,m'}(t;L_2 + 2mL) + U_{m',m'}(t;L_3 + 2mL) \Big] \tag{B.4}$$

where $m' = m+1$ and

$$U_{n,m}(t,x) = \int_{-\infty}^{\infty} \frac{\Gamma_{t_1}^n \Gamma_{t_2}^m}{\omega} e^{-i\omega(t-t_o-\frac{x}{c})} d\omega \tag{B.5}$$

Once the terminal loads Z_{t_1} and Z_{t_2} are given, the integral in (B.5) can be evaluated analytically. It is worthy to note that the expression in (B.4), obtained for an ends-loaded transmission line is also valid for a center-loaded line ($Z_{t_1} = Z_\ell$, $Z_{t_2} = Z_t$) provided that the source or the observation point is located at the center (see Figures 1-c and 1-d).

Time-domain solutions (B.4) and (12), obtained by two different methods must be equivalent, since both are the solutions of the same differential equation. For early times first term in (B.4) gives the total current, while in (12) many terms are needed for an accurate result. For late times however, the summation in (12) converges very fast and is more efficient than that in (B.4).

A "series-method" representation, similar to that in (B.4), could also be obtained for the transient response of a transmission line with an arbitrarily located load. In general, the response of loaded finite

transmission line for the "early times" (i.e., before the first reflected current wave from the ends reaches the observation point) is identical to that of the corresponding infinite line. It can easily be shown that the transient response of a loaded infinite line with the load, $R_\ell - C_\ell$, $R_\ell \| C_\ell$ or $R_\ell - L_\ell$, located at d and the voltage generator, $V_o H(t)$, located at z', is simply given by

$$I_{inf}(t;z,z') = H\left(T - \frac{|z-z'|}{c}\right) \frac{V_o}{R_o(r+1)}\, q(t;z,z') \tag{B.6}$$

where

$$q(t;z,z') = \exp[-\pi(\frac{x_c}{r+1})(T - \frac{|z-z'|}{L})] \quad ; \text{ for } R_\ell - C_\ell \tag{B.7}$$

$$= 1 + r \exp[-\pi(\frac{r+1}{r})\, x_c\, (T - \frac{|z-z'|}{L})]; \text{ for } R_\ell \| C_\ell \tag{B.8}$$

$$= 1 - \exp[-\pi(\frac{r+1}{x_L})(T - \frac{|z-z'|}{L})] \quad ; \text{ for } R_\ell - L_\ell \tag{B.9}$$

wherein

$$T = \frac{ct}{L}\,, \quad r = \frac{R_\ell}{R_o}\,; \quad x_c = (\frac{L}{c\pi})\,\frac{1}{c_\ell}\,; \quad x_L = (\frac{L}{c\pi})\, L_\ell\,.$$

In obtaining (B.6) we have assumed that $z_< \le d \le z_>$ where $z_{\gtrless} = \max_{\min}(z,z')$. The simple expressions in (B.6) to (B.9) can be used together with the SEM representation in (45) to efficiently calculate the transient response of a loaded finite transmission line.